Characterization of the dual functions of *Leishmania* CK1.2 in both the parasite and the macrophage using integrated proteomics and spatial mapping

Daniel MARTEL[1,2], Olivier Leclercq[1,2], Florent Dingli[4], Victor Laigle[4], Damarys Loew[4], Gerald F. SPÄTH[2] and Najma RACHIDI[1,2*].

[1] Institut Pasteur, Université Paris Cité and INSERM U1201, Groupe de signalisation et interactions hôte-parasite, Paris, France; [2] Institut Pasteur, Université de Paris and INSERM U1201, Unité de Parasitologie moléculaire et Signalisation, Paris, France; [3] Laboratoire de Spectrométrie de Masse Protéomique (LSMP), Centre de Recherche, Institut Curie, PSL Research University, Paris, France

Running Title: *The dual function of* Leishmania *CK1.2 in the parasite and its host cell*

*To whom correspondence should be addressed: Najma Rachidi. Institut Pasteur and INSERM U1201, Unité de Parasitologie Moléculaire et Signalisation, Paris, France. Tel: +33144389231; Fax: +330145688332; E-mail: najma.rachidi@pasteur.fr

Keywords: CK1; Interactome; Localisation; Macrophage; *Leishmania*.

Abstract

Leishmania CK1.2 (L-CK1.2) is a serine/threonine protein kinase essential for the survival and immune evasion of the protozoan parasite *Leishmania*, the causative agent of Leishmaniasis. This study investigates the multifaceted roles of L-CK1.2, which exhibits a dynamic localization pattern and a broad spectrum of interacting partners within the parasite. Using proteomic analysis and confocal microscopy, we identified 230 L-CK1.2-associated proteins (L-CKAPs) across the parasite life stages, promastigotes, which replicate within the insect vector, and amastigotes, which proliferate inside the phagolysosomes of host macrophages. This analysis revealed the ubiquitous presence of L-CK1.2 within various cellular structures, including the cytoskeleton, basal body, and flagellum. Our data also identified 64 host proteins (L-CKAP*host*) that interact with L-CK1.2, implicating it in modulating critical host biological processes such as immune response, apoptosis, and purine biosynthesis, processes regulated by *Leishmania* during infection. The study highlights the dual function of L-CK1.2 as it plays roles both in the parasite (cis) and within the host cell (trans), positioning this kinase as a key player in host-pathogen interactions. This work provides a comprehensive map of L-CK1.2 interactions and uncovers its importance in regulating intracellular survival, providing potential therapeutic targets for Leishmaniasis. Furthermore, given the evolutionary conservation of CK1.2 across other parasitic organisms, our findings may have broader implications for understanding and managing parasitic infections.

Introduction

CK1 family members are serine/threonine protein kinases ubiquitously expressed in eukaryotic organisms [1]. They are involved in a wide range of important cellular processes, such as membrane trafficking or vesicular transport from yeast to humans [1]. Due to its broad spectrum of action, CK1 activity and expression are tightly regulated by several mechanisms, including phosphorylation and subcellular sequestration [1]. Indeed, members of the CK1 family are associated with many subcellular structures and organelles through interactions with specific partners ranging from circadian clock to

cytoskeletal elements, [2-7], reflecting the strong interconnection of CK1 localisation and its functions. Defects in regulation, localisation or the introduction of mutations in the CK1 coding sequence are often associated with important diseases like cancer or neurodegenerative diseases [8 9 10]. Regulation of CK1 pathways has also been linked to infectious diseases. For instance, inhibiting host CK1 suppresses yellow fever virus replication [11], highlighting the crucial role of CK1 in host-pathogen interactions.

The protozoan parasite *Leishmania* is the causative agent of Leishmaniasis, a potentially life-threatening disease with at least three distinct clinical forms depending on the species involved: cutaneous, mucocutaneous and the fatal visceral leishmaniasis. *Leishmania* has two developmental stages, an extracellular promastigote stage that proliferates inside the insect vector, and an intracellular amastigote stage that develops and multiplies inside the phagolysosomes of macrophages. The *Leishmania* genome encodes for six CK1 paralogs [12], of which only CK1.2 and CK1.4 are secreted by the parasite and were shown to be essential for parasite survival [13,14]. CK1.2 is released within the host cell as free protein or via extracellular vesicles [15-17]. The adaptation of L-CK1.2 to two distinct cellular environments, driven by the high conservation of its protein sequence in *Leishmania* spp. and strong identity to its human orthologs, suggests that this protein has been shaped by selective pressures acting both on its functions within the host cell [12,18]. Indeed, our previous study identified potential substrates of L-CK1.2 in the macrophage, indicating its ability to regulate multiple host biological processes, such as 'viral & symbiotic interaction', 'actin cytoskeleton organization' and 'apoptosis' [19]. Its dual functions, in *cis* in the parasite and in *trans* in the host macrophage [12,18,19], suggest *Leishmania* CK1.2 (L-CK1.2) as a key player in host-pathogen interactions. Despite its importance in parasite biology and infection, the functions of L-CK1.2 remain poorly understood, beyond its known interactions with and phosphorylation of heat shock proteins within the parasite, and its ability to phosphorylate host targets such as IFNAR1, IFNAR2 (interferon-α/β receptors)[12,13,19-22]. The essential nature of this kinase and its involvement in most cellular functions present major challenges for functional analysis using genetic approaches. To overcome these limitations and gain insights into the cis and trans functions of L-CK1.2, we chose a complementary approach determining and comparing its interactomes in both the parasite and the host cell. Our proteomic analysis unveils a repertoire of 230 interacting partners for L-CK1.2 across both amastigote and promastigote life stages of the parasite, with Gene Ontology enrichment

analyses indicating its ubiquitous nature and multifaceted localization within various organelles. Applying confocal microscopy, we confirmed the localization of L-CK1.2 at these key subcellular sites, including the cytoskeleton, basal body, and flagellum. We further identified 64 host proteins interacting with L-CK1.2, which again are implicated in a wide range of biological processes such as immune response, apoptosis and purine biosynthetic process. These biological processes are also modulated during *Leishmania* infection, strongly indicating the involvement of L-CK1.2 in subverting host cell signalling. We also demonstrated that certain pathways regulated by L-CK1.2 in the parasite are similarly modulated in the host. Collectively, our data provide compelling evidence for the essential role of L-CK1.2, as a central component of the trans-signalling network between *Leishmania* and the macrophage. This dual biological function opens exciting avenues for future research on the co-evolution of parasite and macrophage biology, and the discovery of host-directed therapeutic interventions.

Results

Leishmania CK1.2 displays a pleiotropic localisation and interacts with numerous proteins in promastigotes and in axenic amastigotes

To determine L-CK1.2 localisation, transgenic *L. donovani* Bob (*Ld*Bob) parasites carrying either the empty pLEXSY vector (referred to as 'mock') or pLEXSY-CK1.2-V5-His_6 (referred to as 'CK1.2-V5'), [18] were fixed with paraformaldehyde (PFA). L-CK1.2 was detected as intense punctate staining in the cytoplasm and the flagellum of PFA-fixed promastigotes expressing L-CK1.2-V5 (Figure 1Aa) but not in the corresponding mock control, which only showed weak background fluorescence (Figure 1Ab). The sum of the fluorescence intensity in the body of CK1.2-V5 promastigotes was significantly higher than that of the mock parasites with a p-value below 0.0001 (Figure S1A), indicating that this punctate staining is specific to CK1.2-V5. The heterogeneity of the staining intensity we observed might be due to the lower abundance of the tagged L-CK1.2, that competes with the more abundant endogenous kinase at a given localisation [18]. Similar localisations were also observed for axenic amastigotes (Figure 1Ac). This pleiotropic localization aligns with the diverse functions attributed to this protein kinase

family. However, in the absence of a signal peptide for specific targeting, CK1 family members may primarily depend on protein-protein interactions for their localization [17].

To identify the L-CK1.2 associated proteins (L-CKAP) influencing the regulation, functions or subcellular localisation of this kinase, we used mock or CK1.2-V5-expressing *Ld*Bob cell line [18]. Three independent immuno-precipitations (IP) with logarithmic phase promastigotes (PRO) and axenic amastigotes (axAMA Elution1, E1 & Elution 2, E2) cell lysates were performed using a mouse monoclonal anti-V5 antibody. The eluted proteins were run on SDS-PAGE and analysed by quantitative label-free mass spectrometry. We identified 1081 proteins in promastigote and 516 in amastigote, from which respectively 645 (Figure 1Ba) and 341 (Figure 1Bb&c) were quantified (for the list of all quantified proteins, see Table S1). In addition to L-CK1.2 itself, 84 proteins in PRO and 146 in axAMA (Table S2) were selected as potential L-CKAPs, based on the following criteria: proteins identified with 2 or more distinct peptides, a fold change ratio CK1.2-V5/mock above 2 and a p-value below 0.05 in at least two replicates (Figure 1Ba-c, red square and Table S2), as well as those uniquely identified in CK1.2-V5 by at least 2 peptides or more in at least two replicates (Figure 1Ba-c, "only in CK1-V5" and Table S2). Forty-two L-CKAPs were shared between both parasite stages (Table S2, green). Half of the proteins identified in PRO and two third of those identified in AxAMA were stage-specific interactors of L-CK1.2 in our conditions. The dissimilarity between the two developmental stages becomes even more apparent when considering the enrichment of Gene Ontology (GO) terms associated with protein class (see Figure S1B and Table S3, PANTHER: http://www.pantherdb.org/) or biological processes (see Figure 1C, PANTHER: http://www.pantherdb.org/). In promastigotes, there is an over-representation of terms like 'translational protein' (Figure S1B) and an exclusive representation of 'methylation' and 'ATP metabolic process' (Figure 1C). Conversely, in axenic amastigotes, terms such as 'membrane traffic protein,' 'protein modifying enzyme,' and 'metabolite interconversion enzyme' exhibit a higher representation (Figure S1B & Table S4), while terms such as 'vesicle-mediated transport', 'exocytic process' and 'catabolic processes' (Figure 1C) are exclusive association of axenic amastigotes. These findings shed light on the distinct functional characteristics exhibited by L-CK1.2 in the two stages, which might be linked to specific protein-protein interactions.

L-CK1.2 localisation in *Leishmania* parasites is consistent with that of its interaction partners.

As the important cytoplasmic staining of L-CK1.2-V5 might mask other more specific localisations, promastigotes were treated with 0,125% NP-40 to permeabilise membranes and facilitate the release of the cytoplasmic pool of L-CK1.2, prior to PFA fixation and staining. The treatment conditions were selected after optimisation steps performed to minimise the impact of the detergent on the nucleus and kinetoplast morphology. We used organelle-specific markers for co-localisation with L-CK1.2 and also to demonstrate the integrity of the organelle. We observed organelle-specific signals (i) adjacent to the kinetoplast (Figure 2Aa, CK1.2-V5 & merge, white arrowhead), (ii) in the flagellar pocket region and along the flagellum (Figure 2Aa, CK1.2-V5 & merge, yellow arrowhead and arrow, respectively), as well as (iii) in the Hoechst-unstained region of the nucleus (Figure 2Aa, CK1.2-V5 & merge, white arrow). Similar localisations were observed in axenic amastigotes (Figure 2Ab, CK1.2-V5 & merge). These signals were reproducibly observed in all the samples that were analysed, including those fixed with methanol (as an example: 3 min, Figure S2), suggesting that the observed localisation is not a consequence of fixation processes. The organelle-specific localisation of L-CK1.2 might be due to interactions with specific L-CKAPs. To determine the potential localisation of these interacting partners in an exhaustive manner, we took advantage of the TrypTag (http://tryptag.org/ [23]), a community database providing the localisation of most proteins encoded in the genome of *Trypanosoma brucei* and we assumed that the L-CKAPs would have similar localisations than their syntenic *T. brucei* orthologs. When possible, we confirmed the localisation with the LeishTag database (https://www.leishtag.org/?pageType=landing). A total of 143 L-CKAPs were assigned subcellular localisation using TrypTag (Table S2, column: *T. brucei* & localisation in *T. brucei* orthologs), and 20 using LeishTag (Table S2, column: localisation in *L. mexicana* paralog & *L. mexicana*). The remaining 24 proteins lacked localisation data in both databases, or had no ortholog in *T. brucei*. The Gene Ontology enrichment for Cellular Component of the L-CKAPs was then established using the *T. brucei* orthologs, which are better annotated and Revigo software (http://revigo.irb.hr/ [24]) of Tritrypdb. L-

CKAPs are localised in multiples organelles, including the cytosol, the nucleolus, the basal body, the flagellum, the flagellar pocket, or the nuclear pore complex (Figure 2B & Table S5 (blue for PRO, red for AxAMA and green for both)). In the following paragraphs, we performed co-localisation studies between L-CK1.2 and marker proteins specific for these organelles to validate its pleiotropic localization.

CK1.2 is localised in the granular zone of the nucleolus and redistributed to the mitotic spindle during mitosis.

Forty-eight L-CKAPs have a potential localisation to the nucleolus (Table S2 and S5). Most of L-CK1.2 interacting partners in the nucleolus are involved in translation, with a wide range of 40S and 60S ribosomal proteins, as well as NOP56 [25]. L-CK1.2 is also detected in the nucleolus as judged by Figure 2Aa (CK1.2-V5, white arrow), where CK1.2-V5 is detected in a Hoechst-unstained, sub-nuclear location. To confirm this result, the localisation of CK1.2-V5 in detergent-treated promastigotes was compared to that of L1C6 antibody, which recognises an unknown nucleolar protein [26]. As expected, the L1C6-targeted antigen was detected in the centre of the nucleolus corresponding to the dense fibrillar zone involved in rDNA transcription (Figure 3A, merged image, red staining) [27], confirming the structural integrity of the nucleolus. In contrast, CK1.2-V5 was detected at the periphery of the nucleolus, as dotted staining around L1C6 (Figure 3A, merged image, green staining). This region corresponds to the granular component of the nucleolus, involved in the last steps of rRNA processing and ribosome biogenesis. Our results indicate that CK1.2 might be involved in rRNA processing rather than in rDNA transcription, which is consistent with its interaction with 40S and 60S ribosomal proteins, as well as the NOP56, a nucleolar protein involved in ribosome biogenesis, which orchestrates the correct assembly and the functioning of the box C/D small nucleolar ribonucleoproteins (snoRNPs) [25,28-30]. In addition to NOP56, L-CK1.2 interacts with members of NOP56 complex such as Fibrillarin (box C/D snoRNPs), Hel67 (LSU assembly factors), 60S ribosomal L7 protein, GTP-binding nuclear protein rtb2 and potentially the heat shock protein DNAJ (Figure 3B, [28]). Our interactome provides additional

evidence supporting the localization of L-CK1.2 to the nucleolus and suggests a role for L-CK1.2 in ribosome processing.

The immunofluorescence experiment also unveils an additional function for nucleolar L-CK1.2. In dividing cells, in contrast to the typical segregation pattern observed for nucleolar components exemplified by L1C6 antigen (Figure 3C, red staining, panels a-f, and Figure S3A [31]), CK1.2 staining elongates from a wheel-shaped to a bar-shaped configuration that spans the entire length of the nucleus, following nucleolar elongation (Figure 3C, green staining, panels a-f, and Figure S3A). This localization pattern bears a resemblance to that of the mitotic spindle, and we have evidence suggesting an interaction between L-CK1.2 and α-tubulin, a component of the microtubules (Table S2). To determine whether L-CK1.2 is localised to the spindle during chromosome segregation, we asked whether L-CK1.2 co-localises with tubulin, a component of the spindle. As shown in Figure 3D (merged panels a-d) and Figure S3B, CK1.2-V5 co-localises with tubulin and thus with the mitotic spindle in specific areas, an observation supported by the mPc at or above 0.5 (Figure 3De, mitotic spindle).

During anaphase, CK1.2-V5 accumulates at each end of the elongated mitotic spindle (Figure 3Dc-merge panel, white arrows; Figure S3Bd, white arrows), similarly to the twinfilin-like protein [32]. These findings suggest that *Leishmania* CK1.2 might play a role in regulating chromosome segregation similarly to TbCK1.2 [32,33]. Consistent with this hypothesis, Nucleus and spindle associated protein 2 (LdNuSAP2), a highly divergent ortholog of Saccharomyces ASE1/HumanPRC1/ArabidopsisMAP65 protein family that mediates spindle elongation, was identified in L-CK1.2 interactome [34] alongside eleven interacting partners of NuSAP2, suggesting that L-CK1.2 might be recruited to the spindle as part of the NuSAP2 complex (Figure 3E, [34]). Further investigations will be required to determine the mechanisms by which CK1.2 regulates mitosis.

A closer examination at potential complexes highlighted the specific association of CK1.2 with the nuclear pore complex subunits in a life-stage specific manner (NPC, Figure 2B, grey square). While L-CK1.2 interacts with only four NPC members in promastigotes (Figure S4C (blue squares) and Table S5), it interacts with eighteen NPC subunits in axenic amastigotes (Figure S4C (blue and red squares) and Table S5), including three hypothetical proteins. These proteins, LdBPK_091010.1, LdBPK_100580.1, LdBPK_281740.1, might be novel components of the NPC, as judged by the

localization of their orthologs in *T. brucei* [23]. These L-CKAPs cover most subcomplexes of the NPC but are particularly enriched in the outer ring (Figure S4C), suggesting a tight, life-stage specific interaction between L-CK1.2 and the nuclear pore in axenic amastigotes. Similarly to L-CK1.2, in *Trypanosoma brucei*, CK1.2 interacts with TbNUP158, a member of the outer ring [35] and Hrr25, CK1 ortholog in *S. cerevisiae*, interacts with and phosphorylates NUP53[36].

CK1.2 localises to the basal body and the flagellum.

Based on GO enrichment analysis of cellular component (Figure 2B), 12 L-CKAPs (Table S5) are predicted to locate to (i) the basal body that regulates flagellum duplication, (ii) the tripartite attachment complex (TAC) that links the segregation of the kinetoplasts to that of the basal bodies, or (iii) the transition fibers (TF), critical for flagellum assembly. Most of these interacting proteins were identified either in axenic amastigotes or in both AxAMA and PRO, none were specific of PRO. Several of these L-CKAPs are linked to the regulation of cell division and/or cytokinesis, such as *Leishmania* AKB1 or KHAP2 [13,37,38], while other are members of the Tripartite Attachment Complex (TAC) such as TAC60 [39]. To determine whether L-CK1.2 localizes to these organelles, we selected two markers, centrin-4 to investigate the potential localisation of CK1.2-V5 to the basal body (Figure 4A, CEN, white arrow) and to the bilobe structure (Figure 4A, CEN, yellow arrow), and IFT172 to investigate the potential localisation of CK1.2-V5 to the transition fibers (Figure 4A, IFT172) [40-42]. As shown in Figure 4A panel a, CK1.2-V5 neither co-localises with the kinetoplast DNA, as shown by the mean Pearson correlation coefficient below 0.5 (mPc=0.27 ± 0.164, Figure 4B), nor with the bilobed structure (Figure 4A panel a, yellow arrow and mPc of 0.47 ± 0.074, Figure 4B,). Instead, it co-localises with centrin-4 to the basal bodies (Figure 4A panel a, white arrows and mPc of 0.741 ± 0.050, Figure 4B), and with IFT172 to the transition fibers, as judged by Figure 4A panel b, white arrow and confirmed by an mPc of 0.805 ± 0.06 (Figure 4B), suggesting that L-CK1.2 might regulate flagellum duplication as well as be loaded onto the flagellum. Consistent with this finding, we confirmed the localisation of CK1.2-V5 to the axoneme (IFT172, Figure 4C, Merge and 3D-view), but not to the paraflagellar rod (PFR2, Figure 4D, panel 3). Noticeably, the abundance of L-CK1.2 in the flagellum is lower than that in the body of the parasite, which is consistent with the filtering existing at the entrance of the flagellum [43]. The flagellar localisation

of L-CK1.2, which aligns with published proteomic data from *T. brucei* and *Leishmania mexicana* flagellum [44,45], as well as the identification of 19 flagellar L-CKAP (Table S5, section flagellum, [45]) indicates a potential function for L-CK1.2 in the flagellum. Based on the literature and our findings, *Leishmania* promastigote, alongside *Chlamydomonas reinhardtii* and *Trypanosoma brucei*, is one of the few eukaryotes exhibiting flagellar localization of CK1 [46]. In axenic amastigotes, however, CK1.2-V5 does not colocalise with IFT172, but instead localises around the flagellum (Figure 4E, panel b and 3D view). These findings suggest that the role of CK1.2 in the flagellum is more likely associated with motility or flagellum assembly than its sensing function.

Leishmania CK1.2 interacts with host proteins.

L-CK1.2 is secreted into the macrophage via extracellular vesicles, and we and others have shown that it phosphorylates host targets, suggesting it might also interact with host proteins to perform its immune-subversive functions [15,19,22]. To investigate this hypothesis, we employed a method previously described for *Mycobacterium*, as classical immunoprecipitation from *Leishmania*-infected macrophages was technically challenging. The large quantity of material required was incompatible with bone marrow-derived macrophages (BMDM) infected with splenic and liver parasites obtained from *Leishmania*-infected hamsters.

Recombinant L-CK1.2-V5, produced in *E. coli*, was incubated overnight with macrophage protein lysates and immunoprecipitated using an anti-V5 antibody [18,47] to identify the host L-CK1.2-associated proteins (L-CKAP*host*) by mass spectrometry analysis. Two controls were added, an empty vector, and a control-thioredoxin (an empty plasmid expressing thioredoxin-V5), as recombinant L-CK1.2-V5 is fused to thioredoxin at the N-terminus to improve its solubility. Three independent immuno-precipitations were performed using a mouse monoclonal anti-V5 antibody. The proteins were run on SDS-PAGE (Figure 5Aa) and the binding partners revealed by quantitative label-free mass spectrometry (Figure 5Aa, b &c). We identified 64 L-CKAP*host* in at least two replicates with at least two distinct peptides detected (Table S6). L-CK1.2-V5 interacts with a wide range of host protein classes, including chaperones and transporters, similar to the L-CKAPs identified in *Leishmania* (Figure 5B). This

suggests that L-CK1.2 may perform similar functions in both the parasite and its host cell. The GO analysis for Biological Process (Figure S5A) revealed a significant enrichment for the terms 'purine biosynthetic process', 'glycolytic process' (ATP-dependent 6-phosphofructokinase, Pfkl and Glyceraldehyde-3-phosphate dehydrogenase, GAPDH), 'mitochondrial electron transport' (mitochondrial ATP synthase subunit, Atp5f1a, Atp5f1c and Atp5po, Cytochrome b-c1 complex subunit 8) and 'mitochondrial membrane respiratory chain' (Ndufa1, Ndufa10). These findings collectively suggest a potential role for L-CK1.2 in reprogramming host cell energy metabolism, which indeed undergoes a gradual shift from an M2-like respiratory metabolic state to an M1-like glycolytic energy profile during *Leishmania* infection [48]. We also identified an enrichment of GO terms associated with infection, such as "immune response activation," "apoptotic cell death," and "response to stress", indicating a role for L-CK1.2 in subverting key host pathways that enable the parasite to establish its niche and promote intracellular survival (Figure S5A, [49]).

Notably, many of the biological processes enriched in the interactome are also present in the L-CK1.2-related host substratome we previously published (Figure S5B, Table S8 [19]). The most common biological processes shared between the host interactome and the host substratome are related to post-transcriptional regulation processes (Figure S5B, Table S8 [19]). Because of its dual role, L-CK1.2 has the ability to function in both the parasite and the macrophage. To determine whether L-CK1.2 targets the same pathways in both organisms, we analysed the intersection between biological processes associated with L-CK1.2 in the parasite and the host cell by combining the L-CKAP*host* and substratome datasets (this work and [19], Figure 5C, Table S7). Several biological processes were conserved in both organisms, representing the core of L-CK1.2 functions: (i) biosynthetic metabolic processes including RNA metabolic process and lipid biosynthetic process; (ii) translation; (iii) transport including endocytosis, and trafficking; (iv) response to stimuli, regulation of cell communication and signalling (Figure 5C). Another characteristic, conserved in both organisms, is protein folding, through the interaction of L-CK1.2 with chaperone proteins (Figure 5B). We have shown that L-CK1.2 interacts with *Leishmania* chaperone proteins, including HSP70s, HSP60, DNAJs, HSP110 (this work). Similarly in the macrophage, L-CK1.2 interacts with DNAJs, HSPA5 (HSP70) and HSP90. Interestingly, while *Leishmania* HSP90 is phosphorylated by L-CK1.2 [20], only host HSP90 seems to interact with L-CK1.2.

Next, to determine whether L-CK1.2 targets specific pathways in the parasite, we compared the biological processes associated with L-CK1.2 in the parasite and the host cell by combining the L-CKAP*host* and substratome datasets and retained those specific to the parasite (this work and [19], Figure S5C, Table S9). The GO terms for several biological processes are specifically enriched in the L-CK1.2 parasite interactome, including 'precursor large subunit ribosomal RNA maturation', 'TOR signalling' or 'cell cycle regulation' (Figure S5C, Table S9). Further investigations will be needed to determine whether this specificity might arise from interactions with proteins absent in the host or from differences in regulatory mechanisms.

DISCUSSION

Currently, little is known about *Leishmania* CK1.2, despite its crucial role in parasite survival and its validation as a drug target [13,18,50]. Our findings shed light on the versatile and essential nature of L-CK1.2, demonstrated by its diverse subcellular localization and broad spectrum of interacting partners. We showed that the known localisation of L-CK1.2 interacting partners is consistent with L-CK1.2 distribution, suggesting that these proteins may confer the necessary specificity for its functions. This spatial coordination is particularly important given that L-CK1.2 is constitutively active [18]. We unveiled critical roles for L-CK1.2 in the parasite, including its involvement in translational regulation, as evidenced by its interactions with numerous ribosomes, its localisation at the nucleolar periphery, and its potential role in regulating molecular transport across the nuclear envelope. Additionally, specifically in axenic amastigotes, L-CK1.2 might play a role in vesicular trafficking, particularly endocytosis through its interaction with AP2 adaptor protein complex. We are currently investigating this hypothesis.

We also identified host biological processes that may be regulated by L-CK1.2 through interactions with host proteins, providing insight into its role during infection. Many of the enriched host processes in our dataset, including cell death, immune response, and transport, are known to be modulated during *Leishmania* infection [51-54]. The two main host processes targeted by L-CK1.2 are 'purine biosynthesis'', more specifically linked to 'glycolytic process', and mitochondrial electron transport', indicating the potential involvement of L-CK1.2 in the regulation of the host respiratory metabolism. This finding is

consistent with recent data from Zhang *et al.* showing that macrophages infected with *Leishmania amazonensis* shift towards aerobic glycolysis for ATP production [48]. Second, we identified many proteins linked to mitochondrial electron transport, particularly from the complex I, such as Ndufa10, Ndufs1 and Ndufs3, subunits of the mitochondrial membrane respiratory chain NADH dehydrogenase, important to maintain the mitochondrial membrane potential. *Leishmania* is known to target host mitochondria to modulate survival and also to control mitochondrial bioenergetics [55]. Consistent with a role for L-CK1.2 in this process during *Leishmania* infection, human CK1δ/CK1ε have been shown to be involved in the regulation of complexes I and IV of the electron transport chain [56].

The release of L-CK1.2 in the host cell via extracellular vesicles, as well as its ability to interact with and phosphorylate host proteins, suggest a dual role for L-CK1.2, in both the parasite and the host cell to regulate intracellular parasite survival (this work, [15,19,22]). Unlike viruses or bacteria that hijack host CK1 to manipulate cellular functions, *Leishmania* secretes its own CK1, suggesting that L-CK1.2 can functionally replace its mammalian counterparts. Supporting this hypothesis, our previous work demonstrated that the first 325 of the 353 amino acids, encompassing the catalytic domain and part of the C-terminus, are fully conserved among human-infecting *Leishmania* species, establishing L-CK1.2 as the most conserved kinase across these parasites [18]. This conservation, unaffected by geographical diversity or differences in insect vectors, is likely driven by strong selective pressure from mammalian host cells on the L-CK1.2 protein sequence, explaining its high similarity to human orthologs [12,18]. However, this similarity does not extend to the C-terminus, suggesting that this domain might not be important for L-CK1.2 host functions. This hypothesis is not supported by the high conservation of L-CK1.2 C-terminal domain in most *Leishmania* species infecting humans [12,18]. One possible explanation lies in the presence of Low Complexity Regions (LCRs) within this domain. LCRs have been shown to be more abundant in highly connected proteins, such as signaling kinases, and contribute to protein interactions [57]. Notably, LCRs are also found in the C-terminal domains of human CK1α, CK1δ, CK1ε, CK1γ1, CK1γ2, and CK1γ3 (Figure S6, http://smart.embl-heidelberg.de/smart/set_mode.cgi?NORMAL=1, [58]). This conservation is striking, given the divergence of the L-CK1.2 C-terminus from its mammalian counterparts, suggesting that LCRs may be the key

elements enabling L-CK1.2 to recognize proteins in the parasite and in the host. These protein-protein interactions are crucial, as L-CK1.2 is devoid of signal peptide or any similar domains [12,18], and thus likely relies on host interacting partners to reach its subcellular localisation to exert its functions, like its mammalian orthologs[17]. Conceivably, blocking these interactions will prevent L-CK1.2 functions in the host cell and will likely reduce parasite survival, a possibility we are currently investigating.

Another puzzling question is why *Leishmania* parasites would release an ortholog of kinases already present in the host cell, rather than subvert host CK1 like viruses or bacteria [59,60]? Is L-CK1.2 in competition with the host CK1s? We hypothesize that during *Leishmania* infection, the functions targeted by L-CK1.2 might be attenuated by the inhibition or the reduced abundance of the host CK1s. One publication supports this hypothesis: Isnard *et al.* showed that CK1α, presents in the nucleus of host macrophage, decreases in abundance during *L. major* or *L. mexicana* infection [61]. Interestingly, human CK1α phosphorylates IFNAR1/2 leading to its degradation [19,22] and the removal of the interferon α and β receptor from the plasma membrane. This example shows that during infection while the macrophage would need to decrease CK1α to maintain those receptors at the cell surface and perceive the extracellular environment, the parasite would rather remove them by secreting its own CK1 to ensure that the macrophage is unaware of its environment, thus creating a safe niche for the parasite. Moreover, whereas the mammalian CK1α, CK1δ, and CK1ε are autoinhibited and need the interactions with other proteins, such as DDX3, for its activation, L-CK1.2 does not require interacting partners for its activity [18,62].

One conserved feature of L-CK1.2 between the parasite and the host is its interaction with heat shock proteins, suggesting that L-CK1.2 might particularly contribute to the response to environmental cues. We, as well as other previously published studies, clearly show a strong link between L-CK1.2 and heat shock proteins (Hsps) of the parasite. L-CK1.2 interacts with the *Leishmania* Hsp70s and phosphorylates Hsp23, P23 and Hsp90, (this study, [20,21]. The regulation of Hsp23 and p23 is linked to temperature tolerance, while the phosphorylation of Hsp90 on Ser289 is important for parasite growth, flagella length and morphology [20,21]. Unexpectedly, we did not identify Hsp90 among the L-CKAPs despite its abundance or any proteins involved in the foldosome, such as Sti1 [63]. This finding contrasts

with human CK1s, which phosphorylate Hsp70 and Hsp90 to regulate the balance between protein folding and degradation [64], or whose abundance is regulated by Hsp90 [65]. Noticeably, while L-CK1.2 does not interact with *Leishmania* Hsp90, it interacts with the host Hsp90ab1 (this work and [19]. This suggests that its Hsp90-related functions may differ between the parasite and the macrophage, potentially resembling those of mammalian CK1s more closely. The importance of L-CK1.2 interaction with *Leishmania* Hsp70 is unclear but might be significant. Hsp70 is part of a super family with several paralogs displaying different localisations such as the cytoplasm (HSPA1A), the lumen of the endoplasmic reticulum (HSPA5) or the mitochondrion (HSPA9A) [66]. According to our data, L-CK1.2 interacts with several *Leishmania* Hsp70 paralogs, although assigning a paralog was impossible due to the high percentage of identity between the different members. L-CK1.2 might also interact with host HSPA5, an endoplasmic reticulum chaperone involved in protein folding and quality control.

Our study provides extensive data but has certain limitations, particularly regarding the host dataset, which was derived from macrophage lysates and does not account for localization constraints. Despite this limitation, protein class ontology analysis shows that our host dataset aligns well with the parasite dataset, which was obtained by tagging L-CK1.2 within the parasite. Future research will focus on validating these interactions in more physiological contexts, such as a cellular model or infected macrophages, approaches under active investigation. Tracking the localization of L-CK1.2 in macrophages would be highly informative, though challenging due to its high similarity to host CK1s. We already know that the mouse anti-CK1 antibody cross-reacts with L-CK1.2, and our attempts to use a custom-made L-CK1.2 antibody for immunofluorescence have been unsuccessful. additionally, tagging CK1.2 in the parasite with GFP or similarly sized fluorophores has proven ineffective, as it disrupts kinase function, limiting our options. To overcome these challenges, we are currently developing nanobodies that will be used to specifically follow L-CK1.2 in the host cell and to block its interaction with its host partners.

CONCLUSION

Studying signalling kinases is inherently challenging, as their impairment affects multiple pathways, making it difficult to dissect precise regulatory mechanisms. Our study addresses this challenge by identifying specific interacting partners of L-CK1.2, which was instrumental in elucidating its diverse functions in the parasite (Figure 6). Our findings highlight CK1.2 as a crucial enzyme for both parasite survival and host cell adaptation. The release of L-CK1.2 into the host cell, along with its ability to influence a wide range of host biological processes, positions this kinase as a central driver of macrophage subversion during infection ([15], this work). Furthermore, given the close relationship between *Leishmania* CK1.2 and its orthologs in *Trypanosoma brucei* (TbCK1.2), *Trypanosoma cruzi* (TcCK1.2), *Toxoplasma gondii* (TgCK1α), and *Plasmodium falciparum* (PfCK1) [18], our findings are likely to have broader implications for other parasitic infections.

Materials and Methods

Leishmania cell lines

All the parasite cell lines used in this study were derived from *L. donovani* axenic 1S2D (MHOM/SD/62/1S-CL2D) clone *Ld*Bob, obtained from Steve Beverley, Washington University School of Medicine, St. Louis, MO. Promastigotes were cultured and differentiated into axenic amastigotes as described previously [67]. Parasites cell lines were grown in media with 30 µg/mL hygromycin B (ThermoFisher Scientific Cat# 10687010) to maintain the pLEXSY-CK1.2-V5 or the empty pLEXSY plasmids. The transgenic *L. donovani* cell lines containing either the pLEXSY or pLEXSY-CK1.2-V5-HIS_6 (pLEXSY-CK1.2-V5) vectors, corresponding to the mock or expressing *Leishmania major* CK1.2 tagged with V5 and HIS_6, respectively, were described previously [18]. L-CK1.2-V5 in this strain was shown to be active, functional, able to rescue a decrease in the activity of endogenous CK1.2 and its ectopic expression did not alter the parasite phenotypes.

Immunofluorescence

To confirm the localisation of CK1.2 inferred from the interactome dataset, we used the *Leishmania donovani* mock and CK1.2-V5 parasites (see Mat & Met and [18]). Although, CK1.2-V5 is expressed

ectopically, its abundant is twice as less as the endogenous CK1.2, precluding the risk of localisation artefact due to overexpression. Logarithmic phase promastigotes or axenic amastigotes (48h after shift at 37°C and pH5.5) were resuspended at $2x10^6$ parasites per mL in Dulbecco's Phosphate Buffer Saline (DPBS) (Gibco) from at least three biological replicates, and 500 µL were added to poly-L-lysine-coated coverslips placed in a 24-well plate. Plates were centrifuged 10 min at 1200 g at room temperature to settle parasites onto the coverslips. For fixation alone, cells were washed three times with DPBS and fixed in 4% paraformaldehyde (PFA) in DPBS for 15 min at room temperature. For cytoskeleton preparation, the protocol was adapted from [68]. Briefly, cells were washed three times with DPBS, treated with 0.125% Nonidet 40 (Fluka BioChemika Cat# 74385) in PIPES buffer (100 mM piperazine-N,N-bis(2-ethanesulfonic acid) (PIPES) pH6.8, 1 mM $MgCl_2$) for 2 minutes at room temperature and washed twice for 5 minutes in PIPES buffer. Cells were fixed in 4% PFA in DPBS for 15 min at room temperature. After PFA fixation, cells were washed three times in DPBS, neutralised 10 min with NH_4Cl (50 mM in DPBS), and washed again three times in DPBS. For the immuno-labelling of PFA-fixed cells or cytoskeleton preparations, the samples were blocked with 10% filtered heat-inactivated fetal calf serum (FCS) containing 0.5 $mg.mL^{-1}$ saponin in DPBS for 30 min at room temperature and then washed for 5 min in DPBS. The cells were then incubated with primary antibodies diluted in DPBS with 0.5% Bovine Serum Albumin (BSA) and 0.5 $mg.mL^{-1}$ saponin for 1h at room temperature. Three washes of 10 min were performed and the secondary antibody diluted in DPBS with 0.5% BSA and 0.5 $mg.mL^{-1}$ saponin was added. After one hour incubation at room temperature in the dark, cells were washed twice for 10 min in DPBS with 0.5% BSA and 0.5 $mg.mL^{-1}$ saponin, and then twice in DPBS. Parasites were incubated with 5 $\mu g.mL^{-1}$ Hoechst 33342 in DPBS for 8 min in the dark, washed twice with DPBS, one time with distilled water, air-dried, then mounted with slides using SlowFade Gold Antifade Mountant (ThermoFisher Scientific Cat# S36937). For methanol fixation, logarithmic phase promastigotes were washed twice in DPBS and resuspended at $2x10^7$ parasites per mL. 10^6 parasites were spread onto poly-L-lysine coated slides and allowed to settle for 30 min in a humid chamber. Parasites were then fixed in methanol at -20°C for 3 minutes and rehydrated for 10 min in DPBS at room temperature. For immuno-labelling of methanol-fixed parasites, samples were blocked with 10% filtered heat-inactivated FCS in DPBS for 15 min at room temperature and washed for 5 min in DPBS. Then the cells were treated

similarly as those fixed by PFA. The antibodies used were: mouse IgG2a anti-V5 tag monoclonal antibody (Thermo Fisher Scientific Cat# R960-25, RRID:AB_2556564) diluted at 1/200 (in PFA and methanol fixed parasites) or at 1/300 (in cytoskeleton preparations); rabbit anti-V5 tag polyclonal antibody (Abcam Cat# ab9116, RRID:AB_307024) diluted at 1/400; rabbit anti-LdCentrin polyclonal antibody (kind gift from Hira L. Nakhasi) diluted at 1/2000 [69]; mouse IgG1 anti-IFT172 monoclonal antibody diluted at 1/200 [70]; mouse anti-PFR2 L8C4 clone antibody diluted at 1/10 [71]; mouse L1C6 anti-TbNucleolus monoclonal antibody diluted at 1/100 (kind gift from Keith Gull [72]); mouse IgG1 anti-α-tubulin monoclonal DM1A antibody (Sigma-Aldrich Cat# T9026, RRID:AB_477593) diluted at 1/400; chicken anti-Hsp70 and chicken anti-Hsp90 antibodies diluted at 1/200 [73]. IgG subclass-specific secondary antibodies coupled to different fluorochromes were used for double labelling: anti-mouse IgG (H+L) coupled to AlexaFluor488 (1/200 (PFA- or methanol-fixed parasites)) or 1/300 (cytoskeleton preparations), Thermo Fisher Scientific Cat# A-21202, RRID:AB_141607)); anti-mouse IgG2a coupled to Cy3 (1/600; Jackson ImmunoResearch Labs Cat# 115-165-206, RRID:AB_2338695); anti-mouse IgG1 coupled to AlexaFluor647 (1/600; Thermo Fisher Scientific Cat# A-21240, RRID:AB_2535809); anti-rabbit IgG (H+L) coupled to AlexaFluor488 (1/400; Thermo Fisher Scientific Cat# A-21206, RRID:AB_2535792); anti-mouse IgG (H+L) coupled to AlexaFluor594 (1/200; Thermo Fisher Scientific Cat# A-21203, RRID:AB_2535789); anti-mouse IgG2a coupled to AlexaFluor488 (1/300; Thermo Fisher Scientific Cat# A-21131, RRID:AB_2535771); anti-mouse IgG1 coupled to AlexaFluor594 (1/300; Thermo Fisher Scientific Cat# A-21125, RRID:AB_2535767); anti-chicken IgY coupled to AlexaFluor594 (1/200; Jackson ImmunoResearch Labs Cat# 703-586-155, RRID:AB_2340378) and anti-rabbit IgG (H+L) coupled to AlexaFluor594 (1/400; Thermo Fisher Scientific Cat# A-21207, RRID:AB_141637).

Confocal microscopy

Images were visualised using a Leica SP5 HyD resonant scanner Matrix screener inverted microscope equipped with a HCX PL APO CS 63x, 1.4 NA oil objective (Leica, Wetzlar, Germany). Triple or quadruple immunofluorescence was imaged with Leica Application Suite AF software (LAS AF; Leica Application Suite X, RRID:SCR_013673) after excitation of the Hoechst 33342 dye with a diode at a

wavelength of 405 nm (452/75 Emission Filter), excitation of the AlexaFluor488 with an argon laser at a wavelength of 488 nm (525/50 Emission Filter), excitation of AlexaFluor594 with a diode DPSS at a wavelength of 561 nm (634/77 Emission Filter), excitation of Cy3 with a diode DPSS at a wavelength of 561 nm (595/49 Emission Filter), and excitation of AlexaFluor647 with a helium-neon laser at a wavelength of 633 nm (706/107 Emission Filter). Images were scanned sequentially to minimise cross excitation between channels and each line was scanned twice and averaged to increase the signal-to-noise ratio. The pinhole aperture was set to 1 airy. Images were acquired with 8x zoom at a resolution of 1024×1024. Z-stacks were acquired at 0.082 µm intervals, deconvolved and rendered using either Fiji (RRID:SCR_002285) or Icy (RRID:SCR_010587) software [74] (http://icy.bioimageanalysis.org/).

Deconvolution of z-stacks and chromatic aberration correction

All confocal images were processed and analysed by using the Huygens Professional software version 19.04 (Scientific Volume Imaging, Huygens Software, RRID:SCR_014237). Deconvolution of confocal z-stacks was optimised using the following settings: automatic estimation of the average background with the mode "Lowest" and area radius = 0.7, deconvolution algorithm CMLE, maximum number of iterations = 40, signal to noise ratio (SNR) = 20, quality change threshold = 0.05, iteration mode = optimised, brick layout = automatic. Theoretical point spread function (PSF) values were estimated for each *z*-stack. All deconvolved images were corrected for chromatic shifts and for rotational differences between different channels using the Chromatic Aberration Corrector (CAC) from Huygens Professional software (Scientific Volume Imaging, Huygens Software, RRID:SCR_014237). To calibrate the image corrections, multifluorescent 0.2 µm TetraSpeck microspheres (ThermoFisher Scientific Cat#T7280) mounted on SlowFade Gold Antifade mountant (ThermoFisher Scientific Cat# S36937) were imaged with identical acquisition parameters. Images were deconvolved similarly and were used to perform the chromatic aberration estimations with the cross-correlation method in CAC software. Corrections were saved as templates and applied for correction of the similarly acquired and deconvolved images in CAC.

Co-localisation analysis of confocal images

Co-localisation analysis was performed with the Co-localisation Analyzer plug-in of the Huygens Professional software (Scientific Volume Imaging, Huygens Software, RRID:SCR_014237, v19.04). Processed cross-section images (deconvolved and corrected for chromatic aberrations) of the parasites were opened with this plug-in and Pearson correlation coefficients (PCC) were calculated for each parasite to quantify co-localisation. A PCC above 0.5 indicates co-localisation. Specific areas of the parasite were cropped from the whole image (basal body area, flagella pocket area, mitotic spindle and reduced mitotic spindle areas, flagellar pocket neck area and flagellar tip area) with the "crop" tool of the Huygens Professional software. Criteria to crop specific structures from the images were: (1) basal bodies - a region containing one or two dots representing the basal bodies in the channel CEN and excluding most of the flagellar pocket and flagellar pocket neck; (2) flagellar pocket area – a region stained with CK1.2 and CEN but excluding the basal bodies dots and the flagellum; (3) mitotic spindle – the entire Hoechst-unstained nucleus region in mitotic cells, containing the mitotic spindle in the TUB channel; (4) reduced mitotic spindle areas – only the regions containing the TUB staining in the mitotic nuclei, since CK1.2 is present in Hoechst-unstained regions where TUB staining is not visible, co-localisation of the entire Hoechst-unstained region is biased by a strong staining with CK1.2. We decided to crop further to analyse the colocalisation of CK1.2 and TUB in the mitotic spindle stained by TUB; (5) flagellar pocket neck – a region at the junction of the flagellum and the parasite body, excluding most of the flagellar pocket and basal bodies CK1.2 staining; and (6) flagellar tip – region at the tip of the flagellum, containing only a fraction of the rest of the flagellum. Rationale: since CK1.2 is present in Hoechst-unstained regions where TUB staining is not visible, co-localisation of the entire Hoechst-unstained region is biased by a strong staining with CK1.2. We decided to crop further to analyse the colocalisation of CK1.2 and TUB in the mitotic spindle stained by TUB. For the analysis of the colocalisation of CK1.2 and TUB in the mitotic spindle stained by TUB, we cropped further to restrict to the mitotic spindle as the co-localisation of the entire Hoechst-unstained region was biased by a strong staining with CK1.2. Pearson coefficients were calculated for these images. Pearson coefficients of the co-localisation in the basal body and flagellar pocket areas of (i) CK1.2-V5 with Centrin (CEN), IFT172, and DNA (Hoechst 33342, H); or (i) CEN with IFT172, from 14 images were plotted in

scattered dot plots with the mean and standard deviation using GraphPad Prism 8.1.1 (GraphPad Software, GraphPad Prism, RRID:SCR_002798). Pearson coefficients of the co-localisation of CK1.2-V5 with tubulin in the mitotic spindle and reduced mitotic spindle areas from seven images were plotted similarly. Pearson coefficients of the co-localisation of CK1.2-V5 with Hsp90 from seven images and with Hsp70 from ten images were also plotted similarly.

Epifluorescence microscopy and automated parasite detection

Images were visualised using a Zeiss upright widefield microscope equipped with Apotome2 grids and a Pln-Apo 63x, 1.4 NA oil objective (Zeiss). Light source used was a Mercury Lamp HXP 120, and following filters were used: DAPI (Excitation G365; dichroic FT 395; emission BP 420-470), FITC-A488-GFP (Excitation BP 455-495; dichroic FT 500; emission BP 505-555) and A594-TexasRed-mCherry-HcRed-mRFP (Excitation BP 542-582; dichroic FT 593; emission BP 604-644). Images were captured on an Axiocam MRm camera using ZEN Blue software. For comparison of different cell lines, identical parameters of acquisition were applied on all samples.

Protein extraction, SDS-PAGE and Western blot analysis

Logarithmic phase promastigotes were washed in DPBS and protein extraction was performed as described previously [67]. Ten micrograms of total protein were separated by SDS-PAGE, and transferred onto polyvinylidene difluoride (PVDF) membranes (Pierce). Membranes were blocked with 5% BSA in DPBS supplemented with 0.25% Tween20 (PBST) and incubated over night at 4°C with primary antibody mouse IgG2a anti-V5 tag monoclonal antibody (1/1000; Thermo Fisher Scientific Cat# R960-25, RRID:AB_2556564) in 2,5% BSA in PBST. Membranes were then washed in PBST and incubated with secondary antibody anti-mouse IgG (H+L) coupled to horseradish peroxidase (1/20000; ThermoFisher Scientific Cat# 32230, RRID:AB_1965958). Proteins were revealed by SuperSignal™ West Pico Chemiluminescent Substrate (ThermoFisher Scientific Cat# 34580) using the PXi image analysis system (Syngene) at various exposure times. Membranes were then stained with Bio-Safe Coomassie (Bio-Rad Cat #1610786) to serve as loading controls.

Recombinant expression, purification of CK1.2-V5-His_6 and protein kinase assay

Escherichia coli Rosetta (DE3) pLysS Competent Cells (Merck Cat# 70956) containing pBAD-thio-topo-L-CK1.2-V5-His_6 and pBADthio-V5-His6 (control thioredoxin) were grown at 37°C and induced with arabinose (0,02% final) for 4h at room temperature [18]. Cells were harvested by centrifugation at 10,000 g for 10 min at 4°C and the recombinant proteins were purified as described previously [18 50]. The eluates were supplemented with 15% glycerol and stored at −80°C.

Production of macrophage extracts

Bone marrow derived macrophages (BMDM) were obtained from BALB/c ByJRj mice [75]. Macrophages were lysed with RIPA buffer (150 mM NaCl, 1% Triton X-100, 20 mM Tris HCl [pH 7.4], 1% NP-40, 1 mM EDTA) supplemented with complete protease inhibitor cocktail (Roche Applied Science, IN) and with 1 mM sodium orthovanadate and 1 mM PMSF. Macrophage lysates were then vortexed and, after sonication, clarified by centrifugation.

Immuno-precipitation

Leishmania IP

L. donovani logarithmic phase promastigotes or axenic amastigotes (48h post differentiation) containing either pLEXSY (mock) or pLEXSY-CK1.2-V5-His6 (expressing CK1.2-V5-His6) were collected and total protein were extracted, as described previously [67]. Six (promastigotes) or twelve milligrams (axenic amastigotes) of total proteins were used at 2 mg/mL concentration in RIPA lysis buffer for the immuno-precipitation. The lysates were pre-cleared for 30 min with 1.5 mg of fresh magnetic beads coupled to protein G (ThermoFisher Scientific Cat# 10003D), washed with DPBS-tween buffer (DPBS with 0.02% Tween-20, adjusted at pH 7.4) and mixed with cross-linked anti-V5-coupled magnetic beads according to the manufacturer protocol. After incubation with pre-cleared lysates, beads were washed then the bound proteins were eluted with the glycine elution buffer for the PRO condition and with glycine elution buffer followed by the NuPAGE loading buffer (invitrogen) and heating at 95°C for Ax AMA condition. Elutions were kept at -80°C before mass spectrometry analysis.

Host IP

The rL-CK1.2-V5, the control thioredoxin and the empty vector were incubated overnight with 142 µg BMDM protein lysates. After preclearing, the samples were incubated with magnetic beads coupled to protein G and cross-linked to anti-V5 antibody. Following washing, the immuno-precipitated proteins were eluted first with glycine elution buffer (elution 1 and 2) then with one elution of NuPAGE loading buffer (elution 3). Elutions 1 and 3 were used for MS analysis and proteins from elution 2 were separated on SDS-PAGE and stained with SYPRO Ruby to assess the IP (Figure 5A).

Mass spectrometry analysis

MS analysis of the samples was done at the "Laboratoire de Spectrométrie de Masse Protéomique (LSMP)" platform at Institut Curie in Paris.

Leishmania IP

Proteins were run on SDS–PAGE gels (Invitrogen) without separation just as a clean-up step and stained with colloidal blue staining (LabSafe GEL Blue™ G Biosciences). Gel slices were excised, and proteins were reduced with 10 mM DTT prior to alkylation with 55 mM iodoacetamide. In-gel digestion was performed using trypsin/Lys-C (Promega) overnight in 25 mM NH4HCO3 at 30 °C. Peptides were then extracted using 60/35/5 MeCN/H2O/HCOOH and vacuum concentrated to dryness. Samples were separated by chromatography using an RSLCnano system (Ultimate 3000, Thermo Scientific) coupled to an Orbitrap Fusion mass spectrometer (Q-OT-qIT, Thermo Fisher Scientific). We acquired Survey MS scans in the Orbitrap with the resolution set to a value of 120,000 and a 4×10^5 ion count target. Each scan was recalibrated in real time by co-injecting an internal standard from ambient air into the C-trap. Tandem MS was performed by isolation at 1.6 Th with the quadrupole, HCD fragmentation with normalized collision energy of 35, and rapid scan MS analysis in the ion trap. The MS2 ion count target was set to 10^4 and the max injection time was 100 ms. Only those precursors with charge state 2–7 were sampled for MS2. The dynamic exclusion duration was set to 60s with a 10 ppm tolerance around the selected precursor and its isotopes. The instrument was run in top speed mode with 3 sec cycles.

For identification, the data were searched against the Ld1S2D database (https://www.ncbi.nlm.nih.gov/bioproject/PRJNA396645, GCA_002243465.1) using Sequest HT

through Proteome Discoverer (version 2.4). Enzyme specificity was set to trypsin and a maximum of two missed cleavages was allowed. Oxidized methionine and N-terminal acetylation were set as variable modifications and carbamidomethyl cysteine as fixed modification. The mass tolerances in MS and MS/MS were set to 10 ppm and 0.6 Da, respectively. The resulting files were further processed using myProMS v3.9.3 (https://github.com/bioinfo-pf-curie/myproms, [76]). False-discovery rate (FDR) was calculated using Percolator [77] and was set to 1% at the peptide level for the whole study. Label-free quantification was performed using peptide extracted ion chromatograms (XICs), re-extracted within conditions, and computed with MassChroQ v.2.2.21 [78]. For protein quantification, XICs from proteotypic peptides shared between compared conditions (TopN matching) with missed cleavages were used. Median and scale normalization at peptide level was applied on the total signal to correct the XICs for each biological replicate (N=3 in both conditions). To estimate the significance of the change in protein abundance, a linear model (adjusted on peptides and biological replicates) was performed, and p-values were adjusted using the Benjamini–Hochberg FDR procedure. Proteins with at least two distinct peptides in two replicates of a same state, 2-fold enrichment and an adjusted p-value ≤ 0.05 were considered significantly enriched in sample comparisons. Proteins unique to a condition were also considered if they matched the peptides criteria. The mass spectrometry proteomics raw data have been deposited to the ProteomeXchange Consortium via the PRIDE [79] partner repository with the dataset identifier PXD033809.

Host IP

The elutions 1 and 3 were also run on SDS-PAGE without separation and only one gel slice containing the entire elution fraction was excised and used for nanoscale liquid chromatography coupled to tandem mass spectrometry (nanoLC-MS/MS) as described in the paragraph *Leishmania IP*. For protein identification, the data were searched against the databases containing SwissProt Mus Musculus (16745 sequences), contaminants and Uniprot *L. donovani* CK1.2 by using Sequest HT from Proteome Discoverer (version 2.4 or 2.1). The mass spectrometry proteomics raw data have been deposited to the ProteomeXchange Consortium via the PRIDE [79] partner repository with the dataset identifier: Project accession: PXD064006.

Bioinformatics

The gene ontology analyses were performed with PANTHER (http://www.pantherdb.org/) [80] using *L. major* orthologs as input, or manually annotated using TriTrypDB (https://tritrypdb.org/tritrypdb/app) [81]. STRING database, used to visualize protein complexes among the L-CKAP and L-CKAPhost, were merged to the interaction networks of L-CKAP*host* using Cytoscape software (version 3.7.1, https://string-db.org/) [82]. The localisation of *T. brucei* proteins was determined using TrypTag website (http://tryptag.org/) [23]. The localisation of *Leishmania mexicana* proteins was determined using LeishTag (https://www.leishtag.org/). For motif determination, we used SMART (http://smart.embl-heidelberg.de/). The dataset was analysed for protein-protein interactions and visualized using the STRING plugin (string, https://string-db.org/[83]) of the Cytoscape software package (version 3.8.2, https://cytoscape.org/[84]). Each node represents a substrate, and each edge represents a protein-protein interaction. The text was improved using ChatGPT 3.5 with the prompt, rewrite (version 3.5, https://openai.com/chatgpt).

.

Quantification and statistical analysis

Statistical analyses were performed with GraphPad Prism 8.1.1 (GraphPad Software, GraphPad Prism, RRID:SCR_002798) using unpaired t test (parametric test). Graphs were drawn using the same software. All errors correspond to the 95% confidence interval. Statistically significant differences are indicated with three ($p<0.01$), four ($p<0.001$) or five asterisks ($p<0.0001$). The number of samples analysed for each experiment is indicated in figure legends.

Resource table

REAGENT or RESOURCE	SOURCE	IDENTIFIER
Antibodies		

Anti-V5 tag IgG2a mouse monoclonal	Thermo Fisher Scientific	Cat# R960-25, RRID:AB_2556564
Anti-Centrin from *L. donovani* rabbit polyclonal	[69]	N/A
Anti-IFT172 from *T. brucei* IgG1 mouse monoclonal	[70]	N/A
Anti-V5 tag IgG rabbit polyclonal	Abcam	Cat# ab9116, RRID:AB_307024
Anti-PFR2 from *T. brucei* mouse polyclonal (L8C4)	[71]	N/A
Anti-nucleolus IgG from *T. brucei* mouse monoclonal (L1C6)	Keith Gull, University of Oxford, UK	N/A
Anti-alpha-tubulin IgG1 mouse monoclonal DM1A	Sigma-Aldrich	Cat# T9026, RRID:AB_477593
Anti-mouse IgG (H+L) coupled to AlexaFluor488	Thermo Fisher Scientific	Cat# A-21202, RRID:AB_141607
Anti-mouse IgG2a coupled to Cy3	Jackson ImmunoResearch Labs	Cat# 115-165-206, RRID:AB_2338695
Anti-mouse IgG1 coupled to AlexaFluor647	Thermo Fisher Scientific	Cat# A-21240, RRID:AB_2535809
Anti-rabbit IgG (H+L) coupled to AlexaFluor488	Thermo Fisher Scientific	Cat# A-21206, RRID:AB_2535792
Anti-mouse IgG (H+L) coupled to AlexaFluor594	Thermo Fisher Scientific	Cat# A-21203, RRID:AB_2535789
Anti-mouse IgG2a coupled to AlexaFluor488	Thermo Fisher Scientific	Cat# A-21131, RRID:AB_2535771
Anti-mouse IgG1 coupled to AlexaFluor594	Thermo Fisher Scientific	Cat# A-21125, RRID:AB_2535767

Anti-chicken IgY coupled to AlexaFluor594	Jackson ImmunoResearch Labs	Cat# 703-586-155, RRID:AB_2340378
Anti-rabbit IgG (H+L) coupled to AlexaFluor594	Thermo Fisher Scientific	Cat# A-21207, RRID:AB_141637
Anti-mouse IgG (H+L) coupled to horseradish peroxidase	Thermo Fisher Scientific	Cat# 32230, RRID:AB_1965958
Bacterial Strains		
Escherichia coli Rosetta (DE3) pLysS Competent Cells	Merck	Cat# 70956
Experimental Models: Organisms/Cell lines		
*Ld*Bob cells with pLEXSY vector (mock)	[18]	N/A
*Ld*Bob cells with pLEXSY-CK1.2-V5-His_6 vector, expressing *Lma*CK1.2-V5-His_6	[18]	N/A
Chemicals, Peptides, and Recombinant Proteins		
Nonidet P40 (NP40)	Fluka BioChemika	Cat# 74385
Ammonium Chloride (NH_4Cl)	VWR Chemicals	Cat# 21235.297
Carbobenzoxy-Leu-Leuleucinal (MG132)	Sigma-Aldrich	Cat# M7449
SlowFade Gold Anti-Fade	ThermoFisher Scientific	Cat# S36937
Recombinant thio-*Lma*CK1.2-V5-His_6	[18]	N/A
Recombinant MBP	Sigma-Aldrich	Cat# M1891
Recombinant DNA		
Plasmid: pLEXSY-hyg2 (HygR)	Jena Bioscience	Cat# EGE-232
Plasmid: pLEXSY-CK1.2-V5-His_6 (HygR)	[18]	N/A

Software and Algorithms		
Icy	Icy	RRID:SCR_010587
GraphPad Prism	GraphPad	RRID:SCR_002798
CytExpert Software	Beckman Coulter	RRID:SCR_017217, v2.2.0.97
Fiji	Fiji	RRID:SCR_002285
Huygens Professional	Scientific Volume Imaging	RRID:SCR_014237
Leica Application Suite AF (LAS AF)	Leica	RRID:SCR_013673

Acknowledgments

This work was supported by the ANR-13-ISV3-0009 (to N.R.), by "Région Ile-de-France" and Fondation pour la Recherche Médicale grants (to D.L.). Daniel Martel was supported by the French Government's Investissements d'Avenir program Laboratoire d'Excellence Integrative Biology of Emerging Infectious Diseases (to N.R., grant no. ANR-10-LABX-62-IBEID studentship). The authors would like to thanks Hira L Nakhasi, U.S. FDA, for the anti-*Ld*centrin antibody; Philippe Bastin, Institut Pasteur, for the anti-*Tb*IFT172 and anti-*Tb*PFR2 (L8C4) antibodies; Keith Gull, University of Oxford for the L1C6 antibody; the Unit of Technology and Service - Photonic BioImaging (UTechS PBI) from the Institut Pasteur and the Image Analysis Hub of the Institut Pasteur for the help with confocal microscopy and analyses of co-localisations, in particular Audrey Salles, Julien Fernandes, Anne Danckaert and Jean-Yves Tinevez. Finally, we would like to thank Brice Rotureau, Thierry Blisnick and Philippe Bastin for fruitful discussions and advices.

Author contribution

Conceptualization: NR; Investigation: DM, OL and NR; Formal analysis: DM, OL, FD, VL DL, NR; Writing –original draft: DM, NR; Writing –review & Editing: DM, OL, FD, VL, DL, GFS, NR; Funding acquisition: GFS and NR; Supervision DL and NR.

Figure legends

FIGURE 1: *Leishmania* CK1.2 displays a pleiotropic localisation and interacts with numerous proteins in promastigotes and in axenic amastigotes

(A) IFA of *Ld*Bob pLEXSY-CK1.2-V5 (a) and *Ld*Bob pLEXSY (mock, b) promastigotes, fixed with PFA. The confocal images show the anti-V5 staining (CK1.2-V5 or V5, green), Hoechst 33342 staining (H, blue), a merge and the transmission image (Trans). Scale bar, 2 µm. The pictures are maximum intensity projection of the confocal stacks containing the parasites. (c) IFA of *Ld*Bob pLEXSY-CK1.2-V5 axenic amastigotes, fixed with PFA. The single channel images show CK1.2-V5 (green) and Hoechst 33342 (H, blue) signals, the merge and the transmission image (Trans). Scale bar, 2 µm. The pictures are maximum intensity projection of the confocal stacks containing the parasites. Confocal stacks were deconvolved and corrected for chromatic aberration. The images presented in Figure 1A are representatives of at least 3 replicates. **(B)** Volcano plots representing the changes in protein abundance of LCKAPs in PRO (a), AxAMA elution E1 (b) and E2 (c). Proteins were selected if identified with at least 2 peptides in at least 2 replicates either only in the L-CK1.2-V5 conditions, or with a fold change above 2 and a p-value ≤ 0.05 compared to the mock conditions. **(C)** GO term enrichment for the 'biological process' in promastigotes and axenic amastigotes performed using PANTHER.db (http://www.pantherdb.org/, see also Table S4).

FIGURE 2: L-CK1.2 localisation in *Leishmania* parasites is consistent with that of its interaction partners.

(A) IFA of *Ld*Bob pLEXSY-CK1.2-V5 promastigotes (a) and axenic amastigotes (b) obtained after detergent treatment followed by PFA fixation. Similar to **(Figure 1A)**, except that the images are sum intensity projection of the confocal stacks containing the parasites. The images presented in Figure 2A are representatives of at least 3 replicates. **(B)** Graphical representation of the GO term enrichment for cellular component from the *Trypanosoma brucei* orthologs of both PRO and AxAMA interacting proteins using cytoscape app, Revigo [24] and tritrypdb GO enrichment (https://tritrypdb.org). The dataset of *Trypanosoma brucei* TREU927 has been used. The color of the node represents the (Log10(p-value), between value from - 25.55 to - 1.3). The size of the nodes represents the log size, which is the Log10(Number of annotations for GO Term ID in selected species in the EBI GOA database). Three percent of the strongest GO term pairwise similarities are designated as edges (grey) in the graph [24]. The grey square highlights the nuclear pore complex.

FIGURE 3: CK1.2 localises in the nucleolus and to the mitotic spindle.

(A) IFA pictures of *Ld*Bob pLEXSY-CK1.2-V5 promastigotes obtained after detergent treatment followed by PFA fixation. The images show the single channel images of the transmission image (Trans), CK1.2-V5, Hoechst 33342 (H, blue) and L1C6 signals (red) and merged image. The right panel show a magnification of the nucleus region. Scale bar, 2 µm. These pictures are single stacks extracted from deconvolved confocal stacks corrected for chromatic aberration. **(B)** Subunits of NOP56 complex implicated in ribosomal subunits biogenesis found in our dataset. Fill colors: Green, detected in promastigotes; Yellow, detected in axenic amastigotes; and Green/Yellow, present in both life stage. Border colors: Red, corresponds to box C/D snoRNPs; Purple, corresponds to LSU assembly factors; Blue, putative ribosome assembly factors; and Black, potential interaction found in this study. **(C)** IFA pictures of *Ld*Bob pLEXSY-CK1.2-V5 promastigotes obtained after detergent treatment followed by PFA fixation and stained with anti-V5 (CK1.2-V5) and anti-L1C6 (nucleolus, L1C6) antibodies. Confocal images representing sequential events of mitosis revealed different localisation patterns of L1C6 nucleolar marker and CK1.2-V5. (a – f) The images show the merged image containing CK1.2-

V5 (green), Hoechst 33342 (H) (blue) and L1C6 (red) signals and a magnification of the nuclear region. N=nucleus, K=kinetoplast. Scale bar, 2 µm or 1 µm for magnified images. These pictures are single stacks extracted from deconvolved confocal stacks corrected for chromatic aberration. See also Figure S3A. **(D)** IFA pictures of *Ld*Bob pLEXSY-CK1.2-V5 promastigotes obtained after detergent treatment followed by PFA fixation and stained with anti-V5 and anti-α-tubulin antibodies. Sequential images of various stages of cell division (a – d) showing the single channel images for α-tubulin signals and the merged images showing CK1.2-V5 (green), H (blue) and α-tubulin (red) signals. Scale bar, 2 µm. These pictures are single stacks extracted from deconvolved confocal stacks corrected for chromatic aberration. See also Figure S3B. (e) Dot plots showing Pearson's covariation coefficients for different combination of signals in the entire mitotic spindle region and in a reduced mitotic spindle region containing also CK1.2-V5 signal. Regions of the spindle containing both CK1.2-V5 and tubulin were selected to evaluate whether L-CK1.2 localises to the spindle using Pearson's covariation coefficients. For both regions, CK1.2-V5 signal was compared with α-tubulin (TUB) or Hoechst 33342 (H). The signal of TUB was also compared with H. Pearson's covariation coefficients were measured from n=7 different confocal stacks which were deconvolved and corrected for chromatic aberration with Huygens Professional software. The plot was generated with GraphPad Prism software and the mean values are represented with red bold segments. **(E)** Subunits of NuSAP2 complex, found in our dataset, implicated in chromosome segregation. Fill colors: Green, detected in promastigotes; Yellow, detected in axenic amastigotes; and Green/Yellow, present in both life stage. Border colors: Black, potential interaction found in this study. The images presented in Figure 3 are representatives of at least 3 replicates.

FIGURE 4: CK1.2 is localised to the basal bodies and the flagellum.

(A) IFA of *Ld*Bob pLEXSY-CK1.2-V5 promastigotes obtained after detergent treatment followed by PFA fixation. Single channel images of the CK1.2-V5, Hoechst 33342 (H), centrin 4 (CEN) or IFT172 signals and the transmission image (Trans). The white arrow highlights the basal bodies and the yellow arrow the bilobe region. The merge panel shows CK1.2-V5 signal (green) merged with H (Hoechst 33342, blue), CEN (centrin 4, red) and IFT172 (cyan). The two right panels show a magnification of

region 1 with H signal (blue) merged with (a) CK1.2-V5 (green) and CEN (red) and (b) IFT172 (red) and CK1.2-V5 (green) signals. Scale bar, 2 µm or 1 µm for magnified images. These pictures are single stacks extracted from deconvolved confocal stacks corrected for chromatic aberration. The white arrows highlight the basal bodies and the yellow arrow the bilobe region. **(B)** Dot plots showing Pearson's covariation coefficients in the basal body (BB) or the flagellar pocket (FP) regions for different combination of signals. Pearson's covariation coefficients were measured from n=14 different confocal stacks which were deconvolved and corrected for chromatic aberration with Huygens Professional software. The plot was generated with GraphPad Prism software and the mean values are represented with red bold segments. **(C)** IFA of *Ld*Bob pLEXSY-CK1.2-V5 promastigotes fixed by PFA and stained with the anti-V5 and anti-IFT172 antibodies. The left panels display the single channel images of the CK1.2-V5, IFT172, Hoechst 33342 (H) signals, the transmission image (Trans), and a merge of CK1.2-V5 (green), IFT172 (red) and H (blue) signals. The right panel shows a 3D-reconstruction (3D view) of the flagellum (image 2), with CK1.2-V5 signal (green) merged with IFT172 (red). **(D)** IFA of *Ld*Bob pLEXSY-CK1.2-V5 promastigotes obtained after detergent treatment followed by PFA fixation and staining with the anti-V5 and anti-PFR2 antibodies. The following images show CK1.2-V5, PFR2, Hoechst 33342 (H) signals, the transmission image (Trans), and finally the merge of CK1.2-V5 (green), PFR2 (red) and H (blue) signals. (image 3) 3D-reconstruction (3D view) of the flagellum (white square in (merge)), showing CK1.2-V5 signal (green) merged with PFR2 (red). Scale bars, 2 µm or 1 µm for 2D images. Pictures in (E) and (D, left panels) are single stacks extracted from deconvolved confocal stacks corrected for chromatic aberration. All confocal stacks containing the parasite were used for pictures (D, image 2 and E image 3). **(E)** IFA of *Ld*Bob pLEXSY-CK1.2-V5 axenic amastigotes obtained after detergent treatment followed by PFA fixation. The single channel and the merge images show CK1.2-V5, Hoechst 33342 (H, blue), centrin 4 (CEN, red) or IFT172 (cyan) signals and the transmission image (Trans). Scale bar, 2 µm. These pictures are single stacks extracted from deconvolved confocal stacks corrected for chromatic aberration. Panel a shows a merged of CK1.2-V5, Hoechst 33342 (H, blue) and centrin 4 (CEN, red); Panel b shows CK1.2-V5, Hoechst 33342 (H, blue), and IFT172 (cyan) signals; 3D-reconstruction of the flagellar pocket region and its neck from image

(Figure 5Fa and b), which has been rotated. All confocal z-stacks containing the parasite were used for the 3D view. The images presented in Figure 4 are representatives of at least 3 replicates.

FIGURE 5: L-CK1.2 interacts with macrophage proteins.

(A) The recombinant L-CK1.2-V5, the control-thioredoxin and the control were incubated overnight with BMDM protein lysates and immunoprecipitated using an anti-V5 antibody. The proteins were eluted by two successive elutions with glycine elution buffer (elution 1 and 2) followed by one elution with NuPAGE loading buffer (elution 3). Proteins from elutions 1 and 3 were used for MS analysis (Figure 5A a, b and c). Volcano plots representing the changes in protein abundance of L-CK1.2 vs control (a), of L-CK1.2 vs control thioredoxin (b) and of control thioredoxin vs control (c). Proteins were selected if identified with at least 2 peptides in at least 2 replicates either only in the L-CK1.2-V5 conditions, or with a fold change above 2 and a p-value ≤ 0.05 compared to the controls. **(B)** Graphical representation of the affinity purification merged with the string app to visualise protein-protein interactions for host proteins using the cytoscape app. The classification in different categories is based on GO terms enrichment. The colour of the nodes represents the Fold change (see the legend on the figure). **(C)** GO term enrichment for the 'biological process' common between the host cell and *Leishmania donovani* performed using the cytoscape app (see also Table S7).

FIGURE 6: Potential functions of L-CK1.2 in the parasite and in the host cell.

Working model of L-CK1.2 localization and putative functions within both the parasite and the macrophage. The model illustrates the ubiquitous presence of CK1.2 throughout the cell, implying its involvement in multiple cellular processes. This inference is drawn from the diverse array of interacting partners and substrates associated with CK1.2 (this study; [19]). The pleiotropic nature of CK1.2 underlies its indispensable role in parasite survival. In the model, CK1.2 is depicted in red, and potential regulatory pathways mediated by L-CK1.2 are enclosed within a white square.

References

1 Knippschild, U. *et al.* The CK1 Family: Contribution to Cellular Stress Response and Its Role in Carcinogenesis. *Front Oncol* **4**, 96 (2014). https://doi.org:10.3389/fonc.2014.00096

2 Greer, Y. E. *et al.* Casein kinase 1delta functions at the centrosome and Golgi to promote ciliogenesis. *Molecular biology of the cell* **25**, 1629-1640 (2014).

3 Greer, Y. E. & Rubin, J. S. Casein kinase 1 delta functions at the centrosome to mediate Wnt-3a-dependent neurite outgrowth. *J Cell Biol* **192**, 993-1004 (2011). https://doi.org:10.1083/jcb.201011111

4 Peng, Y. *et al.* Interaction of CK1delta with gammaTuSC ensures proper microtubule assembly and spindle positioning. *Molecular biology of the cell* **26**, 2505-2518 (2015b).

5 Bozatzi, P. & Sapkota, G. P. The FAM83 family of proteins: from pseudo-PLDs to anchors for CK1 isoforms. *Biochemical Society transactions* **46**, 761-771 (2018). https://doi.org:10.1042/BST20160277

6 Hu, Y. *et al.* FRQ-CK1 Interaction Underlies Temperature Compensation of the Neurospora Circadian Clock. *mBio* **12**, e0142521 (2021). https://doi.org:10.1128/mBio.01425-21

7 Wolff, S. *et al.* Interaction of casein kinase 1 delta (CK1 delta) with the light chain LC2 of microtubule associated protein 1A (MAP1A). *Biochimica et biophysica acta* **1745**, 196-206 (2005). https://doi.org:10.1016/j.bbamcr.2005.05.004

8 Knippschild, U. *et al.* The casein kinase 1 family: participation in multiple cellular processes in eukaryotes. *Cell Signal* **17**, 675-689 (2005). https://doi.org:S0898-6568(04)00297-9 [pii] 10.1016/j.cellsig.2004.12.011

9 Schittek, B. & Sinnberg, T. Biological functions of casein kinase 1 isoforms and putative roles in tumorigenesis. *Mol Cancer* **13**, 231 (2014).

10 Jiang, S., Zhang, M., Sun, J. & Yang, X. Casein kinase 1alpha: biological mechanisms and theranostic potential. *Cell Commun Signal* **16**, 23 (2018).

11 Bhattacharya, D., Ansari, I. H. & Striker, R. The flaviviral methyltransferase is a substrate of Casein Kinase 1. *Virus Res* **141**, 101-104 (2009). https://doi.org:10.1016/j.virusres.2009.01.002

12 Rachidi, N., Knippschild, U. & Späth, G. F. Dangerous Duplicity: The Dual Functions of Casein Kinase 1in Parasite Biology and Host Subversion. *Frontiers in Cellular and Infection Microbiology* **11** (2021). https://doi.org:10.3389/fcimb.2021.655700

13 Baker, N. *et al.* Systematic functional analysis of Leishmania protein kinases identifies regulators of differentiation or survival. *Nat Commun* **12**, 1244 (2021). https://doi.org:10.1038/s41467-021-21360-8

14 Dan-Goor, M., Nasereddin, A., Jaber, H. & Jaffe, C. L. Identification of a secreted casein kinase 1 in Leishmania donovani: effect of protein over expression on parasite growth and virulence. *PloS one* **8**, e79287 (2013).

15 Silverman, J. M. *et al.* An exosome-based secretion pathway is responsible for protein export from Leishmania and communication with macrophages. *J Cell Sci* **123**, 842-852 (2010). https://doi.org:10.1242/jcs.056465

16 Atayde, V. D. *et al.* Exosome secretion by the parasitic protozoan Leishmania within the sand fly midgut. *Cell reports* **13**, 957-967 (2015). https://doi.org:10.1016/j.celrep.2015.09.058

17 Xu, P. *et al.* Structure, regulation, and (patho-)physiological functions of the stress-induced protein kinase CK1 delta (CSNK1D). *Gene* **715**, 144005 (2019). https://doi.org:10.1016/j.gene.2019.144005

18 Rachidi, N. *et al.* Pharmacological assessment defines the Leishmania donovani casein kinase 1 as a drug target and reveals important functions in parasite viability and intracellular infection. *Antimicrob Agents Chemother* **58** (2014). https://doi.org:AAC.02022-13 [pii] 10.1128/AAC.02022-13

19 Smirlis, D. *et al.* Identification of the Host Substratome of Leishmania-Secreted Casein Kinase 1 Using a SILAC-Based Quantitative Mass Spectrometry Assay. *Frontiers in cell and developmental biology* **9**, 800098 (2021). https://doi.org:10.3389/fcell.2021.800098

20 Hombach-Barrigah, A. *et al.* Leishmania donovani 90 kD Heat Shock Protein - Impact of Phosphosites on Parasite Fitness, Infectivity and Casein Kinase Affinity. *Scientific reports* **9**, 5074 (2019). https://doi.org:10.1038/s41598-019-41640-0
21 Kröber-Boncardo, C., Lorenzen, S., Brinker, C. & Clos, J. Casein kinase 1.2 over expression restores stress resistance to Leishmania donovani HSP23 null mutants. *Scientific reports* **10**, 15969 (2020). https://doi.org:10.1038/s41598-020-72724-x
22 Liu, J. *et al.* Mammalian casein kinase 1alpha and its leishmanial ortholog regulate stability of IFNAR1 and Type I interferon signaling. *Mol Cell Biol* **29**, 6401-6412 (2009). https://doi.org:MCB.00478-09 [pii]
10.1128/MCB.00478-09
23 Dean, S., Sunter, J. D. & Wheeler, R. J. TrypTag.org: A Trypanosome Genome-wide Protein Localisation Resource. *Trends in Parasitology* **33**, 80-82 (2017). https://doi.org:10.1016/j.pt.2016.10.009
24 Supek, F., Bosnjak, M., Skunca, N. & Smuc, T. REVIGO summarizes and visualizes long lists of gene ontology terms. *PloS one* **6**, e21800 (2011). https://doi.org:10.1371/journal.pone.0021800
25 Nepomuceno-Mejia, T., Florencio-Martinez, L. E. & Martinez-Calvillo, S. Nucleolar Division in the Promastigote Stage of Leishmania major Parasite: A Nop56 Point of View. *BioMed research international* **2018**, 1641839 (2018). https://doi.org:10.1155/2018/1641839
26 Názer, E. & Sánchez, D. O. Nucleolar Accumulation of RNA Binding Proteins Induced by ActinomycinD Is Functional in Trypanosoma cruzi and Leishmania mexicana but Not in T. brucei. *PloS one* **6**, e24184 (2011). https://doi.org:10.1371/journal.pone.0024184
27 Motta, M. C. M., Souza, W. d. & Thiry, M. Immunocytochemical detection of DNA and RNA in endosymbiont-bearing trypanosomatids. *FEMS Microbiology Letters* **221**, 17-23 (2003). https://doi.org:10.1016/S0378-1097(03)00087-9
28 Nepomuceno-Mejia, T., Florencio-Martinez, L. E., Pineda-Garcia, I. & Martinez-Calvillo, S. Identification of factors involved in ribosome assembly in the protozoan parasite Leishmania major. *Acta Trop* **228**, 106315 (2022). https://doi.org:10.1016/j.actatropica.2022.106315
29 Kiss-Laszlo, Z., Henry, Y., Bachellerie, J. P., Caizergues-Ferrer, M. & Kiss, T. Site-specific ribose methylation of preribosomal RNA: a novel function for small nucleolar RNAs. *Cell* **85**, 1077-1088 (1996). https://doi.org:10.1016/s0092-8674(00)81308-2
30 Galardi, S. *et al.* Purified box C/D snoRNPs are able to reproduce site-specific 2'-O-methylation of target RNA in vitro. *Mol Cell Biol* **22**, 6663-6668 (2002). https://doi.org:10.1128/MCB.22.19.6663-6668.2002
31 Ogbadoyi, E., Ersfeld, K., Robinson, D., Sherwin, T. & Gull, K. Architecture of the Trypanosoma brucei nucleus during interphase and mitosis. *Chromosoma* **108**, 501-513 (2000).
32 Kumar, G., Kajuluri, L. P., Gupta, C. M. & Sahasrabuddhe, A. A. A twinfilin-like protein coordinates karyokinesis by influencing mitotic spindle elongation and DNA replication in Leishmania. *Mol Microbiol* **100**, 173-187 (2016). https://doi.org:10.1111/mmi.13310
33 Urbaniak, M. D. Casein kinase 1 isoform 2 is essential for bloodstream form Trypanosoma brucei. *Molecular and Biochemical Parasitology* **166**, 183-185 (2009). https://doi.org:10.1016/j.molbiopara.2009.03.001
34 Zhou, Q. *et al.* Faithful chromosome segregation in Trypanosoma brucei requires a cohort of divergent spindle-associated proteins with distinct functions. *Nucleic acids research* **46**, 8216-8231 (2018). https://doi.org:10.1093/nar/gky557
35 Moreira, C. *et al.* Impact of inherent biases built into proteomic techniques: Proximity labeling and affinity capture compared. *J Biol Chem* **299**, 102726 (2023). https://doi.org:10.1016/j.jbc.2022.102726
36 Lusk, C. P. *et al.* Nup53p is a target of two mitotic kinases, Cdk1p and Hrr25p. *Traffic* **8**, 647-660 (2007).
37 Inoue, M. *et al.* Identification and characterization of a cell division-regulating kinase AKB1 (associated kinase of Trypanosoma brucei 14-3-3) through proteomics study of the Tb14-3-3 binding proteins. *Journal of biochemistry* **158**, 49-60 (2015). https://doi.org:10.1093/jb/mvv018

38 Kelly, F. D. *et al.* A cytoskeletal protein complex is essential for division of intracellular amastigotes of Leishmania mexicana. *J Biol Chem* **295**, 13106-13122 (2020). https://doi.org:10.1074/jbc.RA120.014065
39 Kaser, S. *et al.* Biogenesis of the mitochondrial DNA inheritance machinery in the mitochondrial outer membrane of Trypanosoma brucei. *PLoS pathogens* **13**, e1006808 (2017). https://doi.org:10.1371/journal.ppat.1006808
40 Vaughan, S. & Gull, K. Basal body structure and cell cycle-dependent biogenesis in Trypanosoma brucei. *Cilia* **5**, 5 (2015).
41 Selvapandiyan, A. *et al.* Centrin1 Is Required for Organelle Segregation and Cytokinesis in Trypanosoma brucei. *Molecular Biology of the Cell* **18**, 3290-3301 (2007). https://doi.org:10.1091/mbc.e07-01-0022
42 Shi, J. *et al.* Centrin4 coordinates cell and nuclear division in T. brucei. *Journal of cell science* **121**, 3062-3070 (2008).
43 Bertiaux, E. & Bastin, P. Dealing with several flagella in the same cell. *Cell Microbiol* **22**, e13162 (2020). https://doi.org:10.1111/cmi.13162
44 Subota, I. *et al.* Proteomic analysis of intact flagella of procyclic Trypanosoma brucei cells identifies novel flagellar proteins with unique sub-localization and dynamics. *Molecular & cellular proteomics : MCP* **13**, 1769-1786 (2014). https://doi.org:10.1074/mcp.M113.033357
45 Beneke, T. *et al.* Genetic dissection of a Leishmania flagellar proteome demonstrates requirement for directional motility in sand fly infections. *bioRxiv*, 476994 (2018). https://doi.org:10.1101/476994
46 Boesger, J., Wagner, V., Weisheit, W. & Mittag, M. Application of phosphoproteomics to find targets of casein kinase 1 in the flagellum of chlamydomonas. *International journal of plant genomics* **2012**, 581460 (2012). https://doi.org:10.1155/2012/581460
47 Bach, H., Papavinasasundaram, K. G., Wong, D., Hmama, Z. & Av-Gay, Y. Mycobacterium tuberculosis virulence is mediated by PtpA dephosphorylation of human vacuolar protein sorting 33B. *Cell Host Microbe* **3**, 316-322 (2008). https://doi.org:10.1016/j.chom.2008.03.008
48 Zhang S., L. L., Varet H., Legendre R., Mahtal N., Proux C., Aulner N., Shorte S., Granjean C., Bousso P., Prina E., Späth G.F. The m6A reader IGF2BP2 directs immune-metabolic reprogramming in Leishmania amazonensis-infected macrophages. *bioRxiv* (June 2024). https://doi.org:10.1101/2022.09.08.507100
49 Smirlis, D. *et al.* SILAC-based quantitative proteomics reveals pleiotropic, phenotypic modulation in primary murine macrophages infected with the protozoan pathogen Leishmania donovani. *Journal of proteomics* **213**, 103617 (2020). https://doi.org:10.1016/j.jprot.2019.103617
50 Durieu, E. *et al.* From Drug Screening to Target Deconvolution: a Target-Based Drug Discovery Pipeline Using Leishmania Casein Kinase 1 Isoform 2 To Identify Compounds with Antileishmanial Activity. *Antimicrobial Agents and Chemotherapy* **60**, 2822-2833 (2016). https://doi.org:10.1128/AAC.00021-16
51 Gupta, P., Srivastav, S., Saha, S., Das, P. K. & Ukil, A. Leishmania donovani inhibits macrophage apoptosis and pro-inflammatory response through AKT-mediated regulation of beta-catenin and FOXO-1. *Cell Death Differ* **23**, 1815-1826 (2016). https://doi.org:10.1038/cdd.2016.101
52 Solano-Galvez, S. G., Alvarez-Hernandez, D. A., Gutierrez-Kobeh, L. & Vazquez-Lopez, R. Leishmania: manipulation of signaling pathways to inhibit host cell apoptosis. *Ther Adv Infect Dis* **8**, 20499361211014977 (2021). https://doi.org:10.1177/20499361211014977
53 Rossi, M. & Fasel, N. How to master the host immune system? Leishmania parasites have the solutions! *Int Immunol* **30**, 103-111 (2018). https://doi.org:10.1093/intimm/dxx075
54 Singh, A. K. *et al.* Proteomic-based approach to gain insight into reprogramming of THP-1 cells exposed to Leishmania donovani over an early temporal window. *Infect Immun* **83**, 1853-1868 (2015). https://doi.org:10.1128/IAI.02833-14
55 Moreira, D. *et al.* Leishmania infantum modulates host macrophage mitochondrial metabolism by hijacking the SIRT1-AMPK axis. *PLoS pathogens* **11**, e1004684 (2015). https://doi.org:10.1371/journal.ppat.1004684

56 Burger, K. L. *et al.* CK1delta and CK1epsilon Signaling Sustains Mitochondrial Metabolism and Cell Survival in Multiple Myeloma. *Cancer Res* **83**, 3901-3919 (2023). https://doi.org:10.1158/0008-5472.CAN-22-2350
57 Coletta, A. *et al.* Low-complexity regions within protein sequences have position-dependent roles. *BMC systems biology* **4**, 43 (2010). https://doi.org:10.1186/1752-0509-4-43
58 Schultz, J., Milpetz, F., Bork, P. & Ponting, C. P. SMART, a simple modular architecture research tool: identification of signaling domains. *Proceedings of the National Academy of Sciences of the United States of America* **95**, 5857-5864 (1998). https://doi.org:10.1073/pnas.95.11.5857
59 Xia, C. *et al.* Casein Kinase 1alpha Mediates the Degradation of Receptors for Type I and Type II Interferons Caused by Hemagglutinin of Influenza A Virus. *J Virol* **92** (2018).
60 Jayaswal, S. *et al.* Identification of Host-Dependent Survival Factors for Intracellular Mycobacterium tuberculosis through an siRNA Screen. *PLoS pathogens* **6**, e1000839 (2010). https://doi.org:10.1371/journal.ppat.1000839
61 Isnard, A. *et al.* Impact of Leishmania infection on host macrophage nuclear physiology and nucleopore complex integrity. *PLoS pathogens* **11**, e1004776 (2015). https://doi.org:10.1371/journal.ppat.1004776
62 Dolde, C. *et al.* A CK1 FRET biosensor reveals that DDX3X is an essential activator of CK1epsilon. *J Cell Sci* **131** (2018). https://doi.org:10.1242/jcs.207316
63 Morales, M. A. *et al.* Phosphoproteome dynamics reveal heat-shock protein complexes specific to the Leishmania donovani infectious stage. *Proceedings of the National Academy of Sciences of the United States of America* **107**, 8381-8386 (2010). https://doi.org:10.1073/pnas.0914768107
64 Muller, P. *et al.* C-terminal phosphorylation of Hsp70 and Hsp90 regulates alternate binding to co-chaperones CHIP and HOP to determine cellular protein folding/degradation balances. *Oncogene* (2012). https://doi.org:onc2012314 [pii] 10.1038/onc.2012.314
65 Sharma, K. *et al.* Quantitative proteomics reveals that Hsp90 inhibition preferentially targets kinases and the DNA damage response. *Molecular & cellular proteomics : MCP* **11**, M111 014654 (2012). https://doi.org:10.1074/mcp.M111.014654
66 Drini, S. *et al.* Species- and Strain-Specific Adaptation of the HSP70 Super Family in Pathogenic Trypanosomatids. *Genome Biol Evol* **8**, 1980-1995 (2016). https://doi.org:10.1093/gbe/evw140
67 Martel, D., Beneke, T., Gluenz, E., Spath, G. F. & Rachidi, N. Characterisation of Casein Kinase 1.1 in Leishmania donovani Using the CRISPR Cas9 Toolkit. *BioMed research international* **2017**, 4635605 (2017). https://doi.org:10.1155/2017/4635605
68 Florimond, C. *et al.* BILBO1 Is a Scaffold Protein of the Flagellar Pocket Collar in the Pathogen Trypanosoma brucei. *PLoS pathogens* **11**, e1004654 (2015). https://doi.org:10.1371/journal.ppat.1004654
69 Selvapandiyan, A. *et al.* Expression of a mutant form of Leishmania donovani centrin reduces the growth of the parasite. *J Biol Chem* **276**, 43253-43261 (2001).
70 Absalon, S. *et al.* Intraflagellar transport and functional analysis of genes required for flagellum formation in trypanosomes. *Mol Biol Cell* **19**, 929-944 (2008). https://doi.org:10.1091/mbc.e07-08-0749
71 Kohl, L., Sherwin, T. & Gull, K. Assembly of the Paraflagellar Rod and the Flagellum Attachment Zone Complex During the Trypanosoma brucei Cell Cycle. *Journal of Eukaryotic Microbiology* **46**, 105-109 (1999). https://doi.org:10.1111/j.1550-7408.1999.tb04592.x
72 Devaux, S. *et al.* Diversification of function by different isoforms of conventionally shared RNA polymerase subunits. *Mol Biol Cell* **18**, 1293-1301 (2007). https://doi.org:10.1091/mbc.e06-09-0841
73 Hombach, A., Ommen, G., Chrobak, M. & Clos, J. The Hsp90–Sti1 interaction is critical for Leishmania donovani proliferation in both life cycle stages. *Cellular Microbiology* **15**, 585-600 (2013). https://doi.org:10.1111/cmi.12057
74 Schindelin, J. *et al.* Fiji: an open-source platform for biological-image analysis. *Nature methods* **9**, 676-682 (2012). https://doi.org:10.1038/nmeth.2019

75 Aulner, N. *et al.* High content analysis of primary macrophages hosting proliferating Leishmania amastigotes: application to anti-leishmanial drug discovery. *PLoS Negl Trop Dis* **7**, e2154 (2013). https://doi.org:10.1371/journal.pntd.0002154
76 Poullet, P., Carpentier, S. & Barillot, E. myProMS, a web server for management and validation of mass spectrometry-based proteomic data. *PROTEOMICS* **7**, 2553-2556 (2007). https://doi.org:10.1002/pmic.200600784
77 The, M., MacCoss, M. J., Noble, W. S. & Kall, L. Fast and Accurate Protein False Discovery Rates on Large-Scale Proteomics Data Sets with Percolator 3.0. *J Am Soc Mass Spectrom* **27**, 1719-1727 (2016). https://doi.org:10.1007/s13361-016-1460-7
78 Valot, B., Langella, O., Nano, E. & Zivy, M. MassChroQ: a versatile tool for mass spectrometry quantification. *Proteomics* **11**, 3572-3577 (2011). https://doi.org:10.1002/pmic.201100120
79 Perez-Riverol, Y. *et al.* The PRIDE database at 20 years: 2025 update. *Nucleic acids research* **53**, D543-D553 (2025). https://doi.org:10.1093/nar/gkae1011
80 Mi, H. *et al.* PANTHER version 16: a revised family classification, tree-based classification tool, enhancer regions and extensive API. *Nucleic acids research* **49**, D394-D403 (2021). https://doi.org:10.1093/nar/gkaa1106
81 Aslett, M. *et al.* TriTrypDB: a functional genomic resource for the Trypanosomatidae. *Nucleic acids research* **38**, D457-462 (2010). https://doi.org:10.1093/nar/gkp851
82 Szklarczyk, D. *et al.* The STRING database in 2023: protein-protein association networks and functional enrichment analyses for any sequenced genome of interest. *Nucleic acids research* **51**, D638-D646 (2023). https://doi.org:10.1093/nar/gkac1000
83 Szklarczyk, D. *et al.* STRING v11: protein-protein association networks with increased coverage, supporting functional discovery in genome-wide experimental datasets. *Nucleic acids research* **47**, D607-D613 (2019). https://doi.org:10.1093/nar/gky1131
84 Shannon, P. *et al.* Cytoscape: a software environment for integrated models of biomolecular interaction networks. *Genome Res* **13**, 2498-2504 (2003). https://doi.org:10.1101/gr.1239303

Figure 1

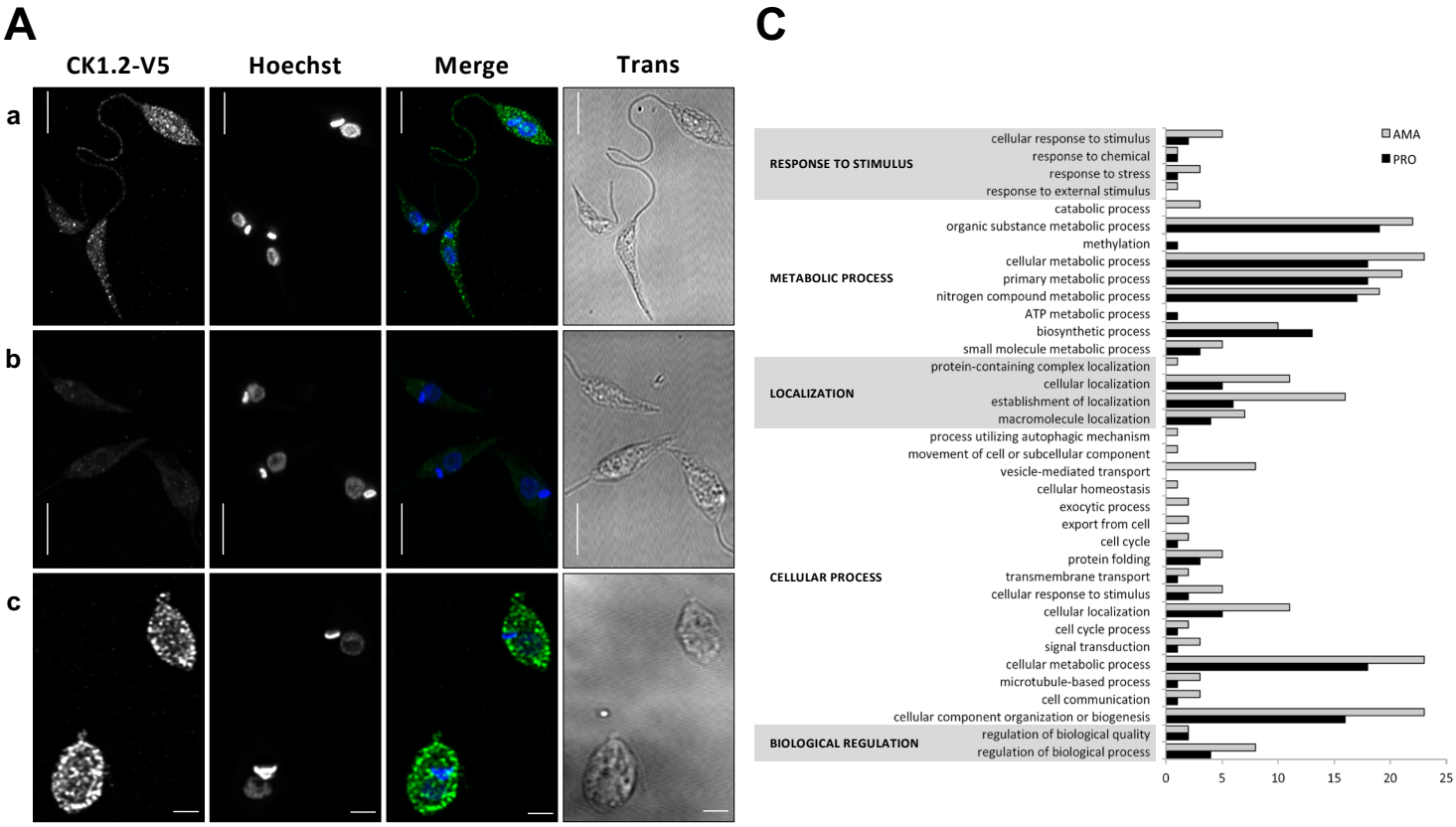
A
CK1.2-V5
Hoechst
Merge
Trans
a
b
c
C
AMA
PRO
RESPONSE TO STIMULUS
cellular response to stimulus
response to chemical
response to stress
response to external stimulus
METABOLIC PROCESS
catabolic process
organic substance metabolic process
methylation
cellular metabolic process
primary metabolic process
nitrogen compound metabolic process
ATP metabolic process
biosynthetic process
small molecule metabolic process
LOCALIZATION
protein-containing complex localization
cellular localization
establishment of localization
macromolecule localization
CELLULAR PROCESS
process utilizing autophagic mechanism
movement of cell or subcellular component
vesicle-mediated transport
cellular homeostasis
exocytic process
export from cell
cell cycle
protein folding
transmembrane transport
cellular response to stimulus
cellular localization
cell cycle process
signal transduction
cellular metabolic process
microtubule-based process
cell communication
cellular component organization or biogenesis
BIOLOGICAL REGULATION
regulation of biological quality
regulation of biological process
0
5
10
15
20
25

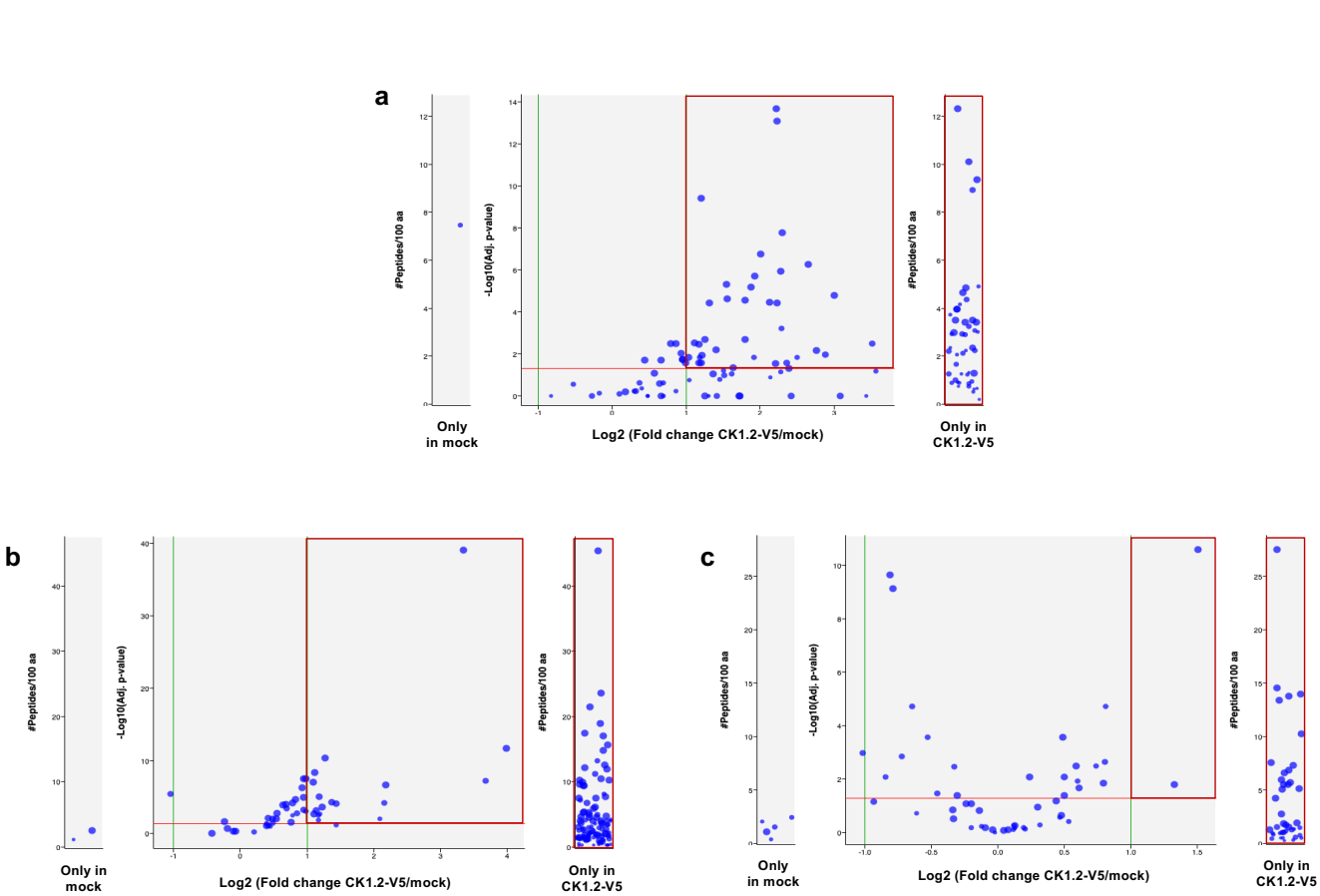
B
a
#Peptides/100 aa
-Log10(Adj. p-value)
Only in mock
Log2 (Fold change CK1.2-V5/mock)
Only in CK1.2-V5
b
c

Figure 2

A

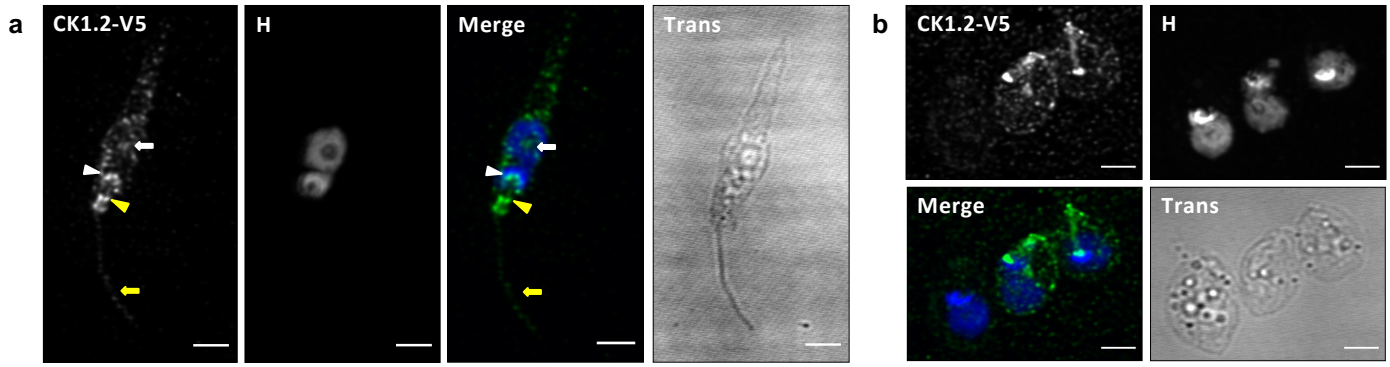
a
CK1.2-V5
H
Merge
Trans
b
CK1.2-V5
H
Merge
Trans

B

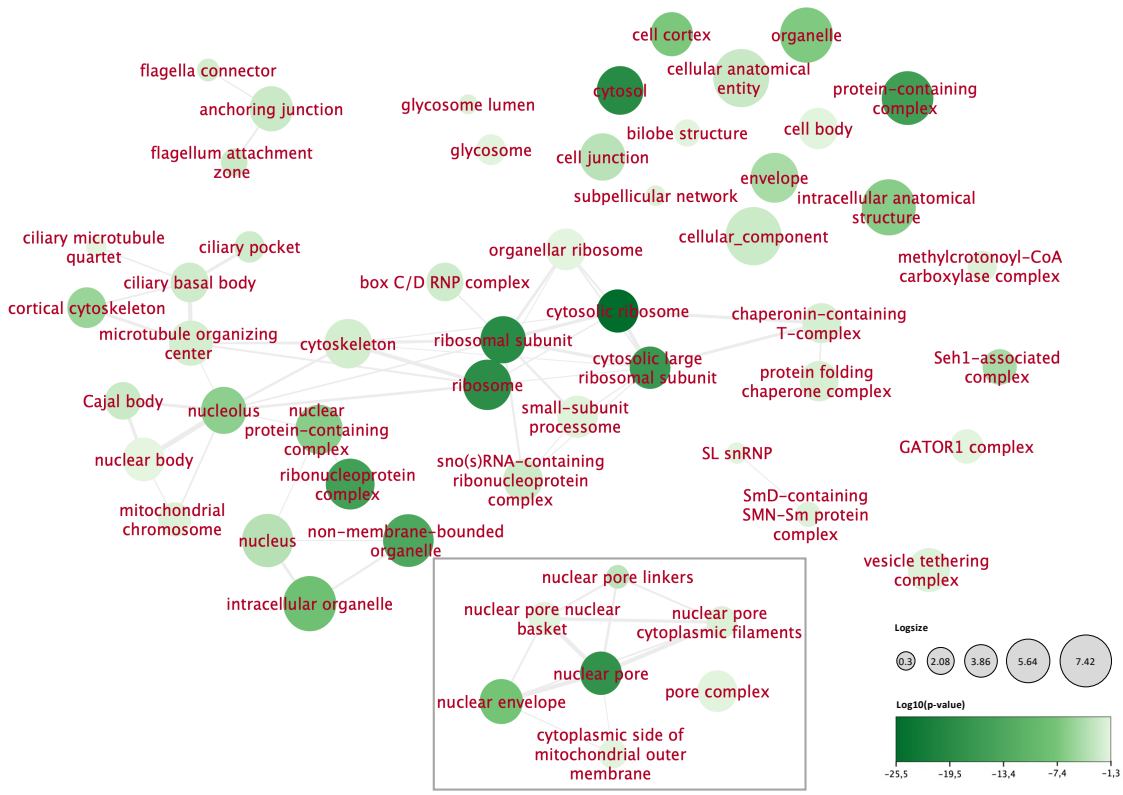
cell cortex
organelle
flagella connector
cellular anatomical entity
cytosol
protein-containing complex
anchoring junction
glycosome lumen
bilobe structure
cell body
flagellum attachment zone
glycosome
cell junction
envelope
subpellicular network
intracellular anatomical structure
ciliary microtubule quartet
ciliary pocket
organellar ribosome
cellular_component
methylcrotonoyl-CoA carboxylase complex
ciliary basal body
box C/D RNP complex
cortical cytoskeleton
cytosolic ribosome
chaperonin-containing T-complex
microtubule organizing center
cytoskeleton
ribosomal subunit
cytosolic large ribosomal subunit
protein folding chaperone complex
Seh1-associated complex
ribosome
Cajal body
nucleolus
nuclear protein-containing complex
small-subunit processome
nuclear body
ribonucleoprotein complex
sno(s)RNA-containing ribonucleoprotein complex
SL snRNP
GATOR1 complex
mitochondrial chromosome
SmD-containing SMN-Sm protein complex
nucleus
non-membrane-bounded organelle
vesicle tethering complex
intracellular organelle
nuclear pore linkers
nuclear pore nuclear basket
nuclear pore cytoplasmic filaments
nuclear pore
nuclear envelope
pore complex
cytoplasmic side of mitochondrial outer membrane
Logsize
0.3
2.08
3.86
5.64
7.42
Log10(p-value)
-25,5
-19,5
-13,4
-7,4
-1,3

Figure 3

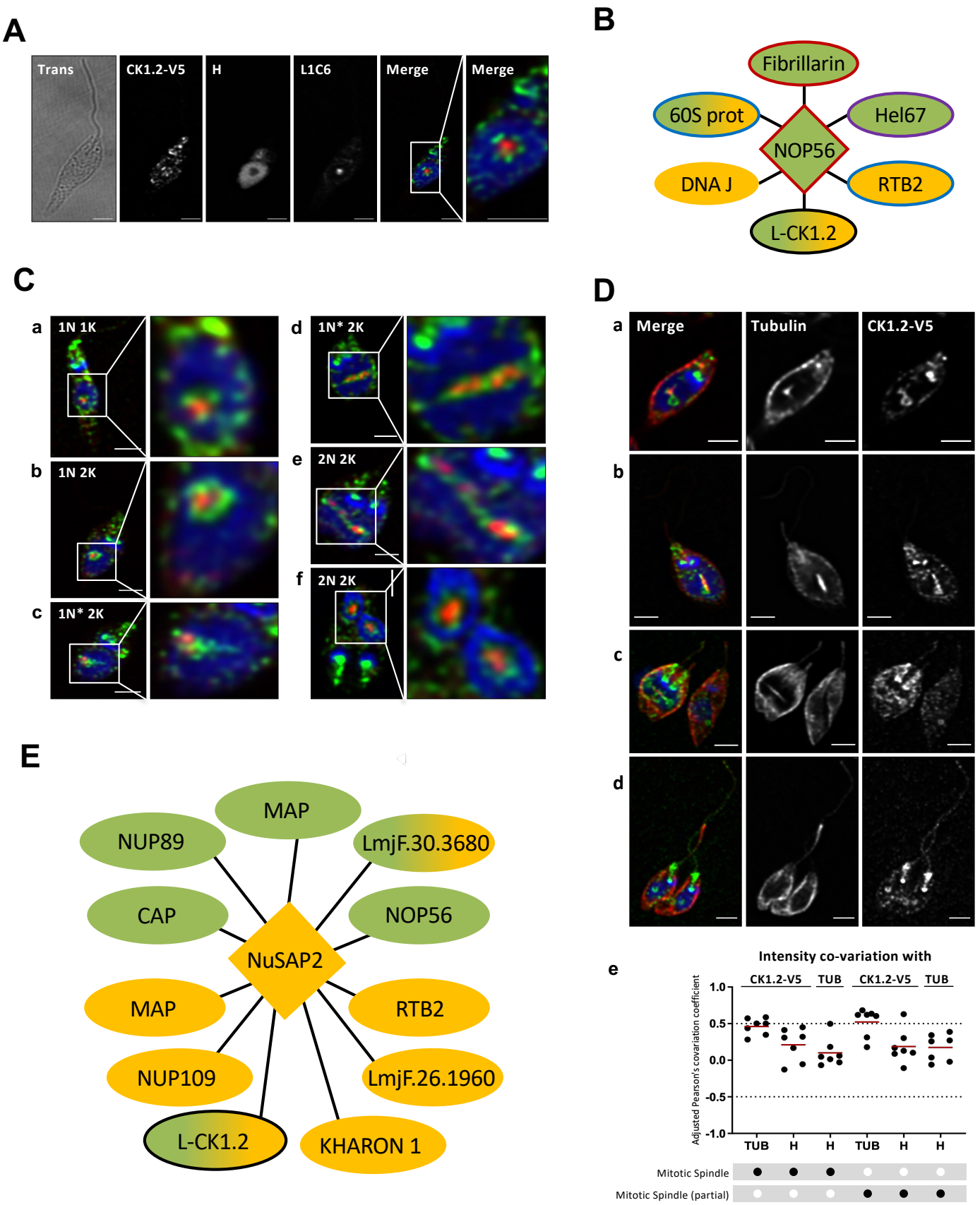
A
Trans
CK1.2-V5
H
L1C6
Merge
Merge
B
Fibrillarin
60S prot
Hel67
NOP56
DNA J
RTB2
L-CK1.2
C
a
1N 1K
b
1N 2K
c
1N* 2K
d
1N* 2K
e
2N 2K
f
2N 2K
D
a
Merge
Tubulin
CK1.2-V5
b
c
d
e
Intensity co-variation with
CK1.2-V5
TUB
CK1.2-V5
TUB
Adjusted Pearson's covariation coefficient
1.0
0.5
0.0
-0.5
-1.0
TUB
H
H
TUB
H
H
Mitotic Spindle
Mitotic Spindle (partial)
E
MAP
NUP89
LmjF.30.3680
CAP
NOP56
NuSAP2
MAP
RTB2
NUP109
LmjF.26.1960
L-CK1.2
KHARON 1

Figure 4

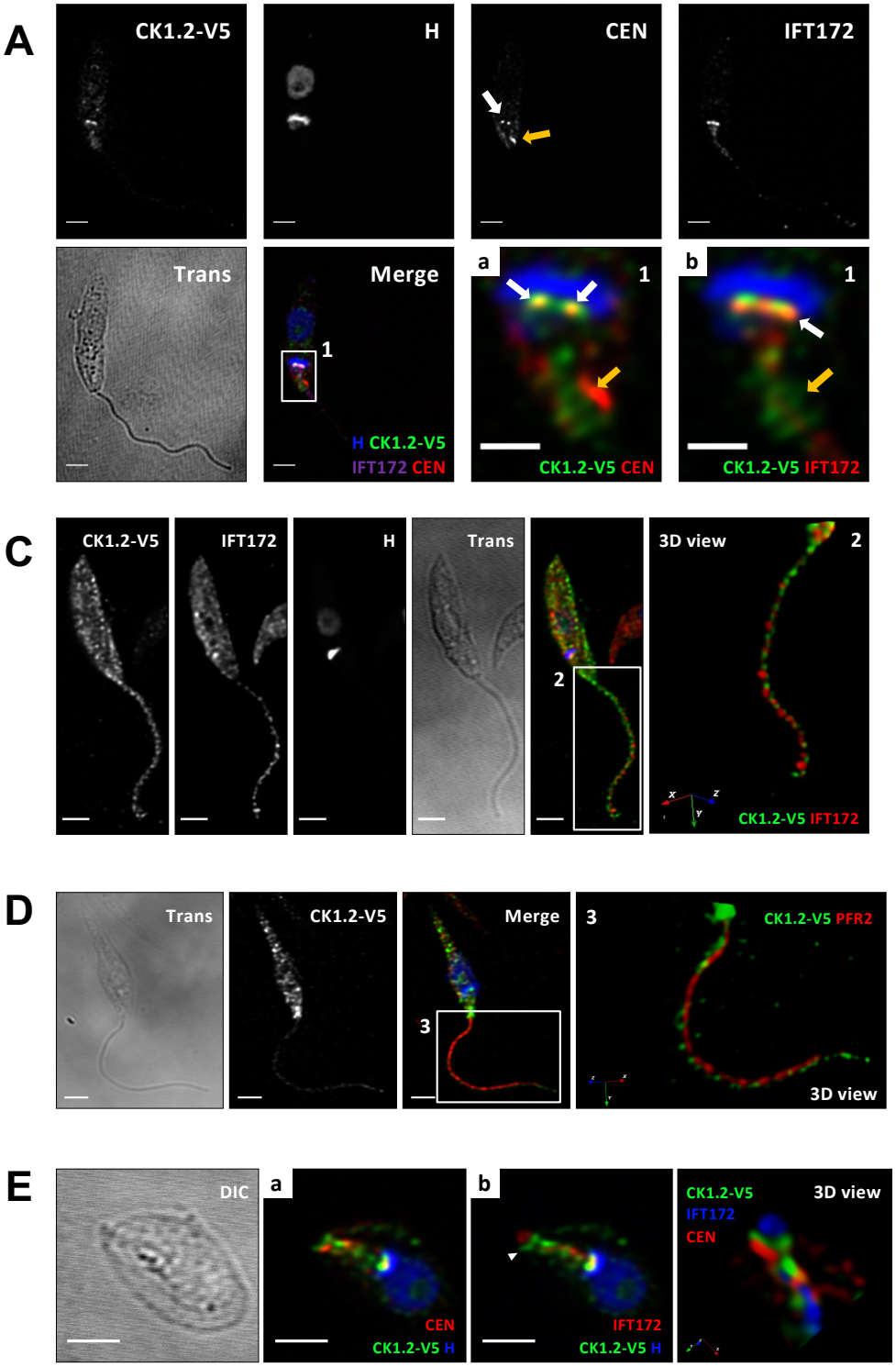
A
CK1.2-V5
H
CEN
IFT172
Trans
Merge
1
H CK1.2-V5
IFT172 CEN
a
1
CK1.2-V5 CEN
b
1
CK1.2-V5 IFT172
C
CK1.2-V5
IFT172
H
Trans
2
3D view
2
CK1.2-V5 IFT172
D
Trans
CK1.2-V5
Merge
3
3
CK1.2-V5 PFR2
3D view
E
DIC
a
CEN
CK1.2-V5 H
b
IFT172
CK1.2-V5 H
CK1.2-V5
IFT172
CEN
3D view

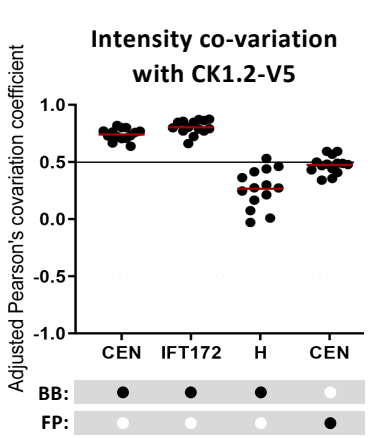
B
Intensity co-variation
with CK1.2-V5
Adjusted Pearson's covariation coefficient
1.0
0.5
0.0
-0.5
-1.0
CEN
IFT172
H
CEN
BB:
FP:

Figure 5

A

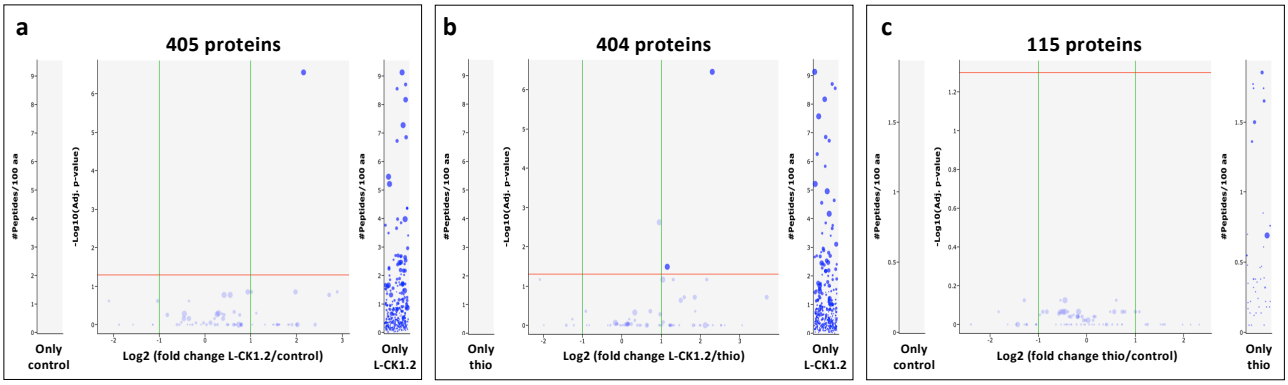
a
405 proteins
#Peptides/100 aa
-Log10(Adj. p-value)
Only control
Log2 (fold change L-CK1.2/control)
Only L-CK1.2
b
404 proteins
Only thio
Log2 (fold change L-CK1.2/thio)
Only L-CK1.2
c
115 proteins
Only control
Log2 (fold change thio/control)
Only thio

B

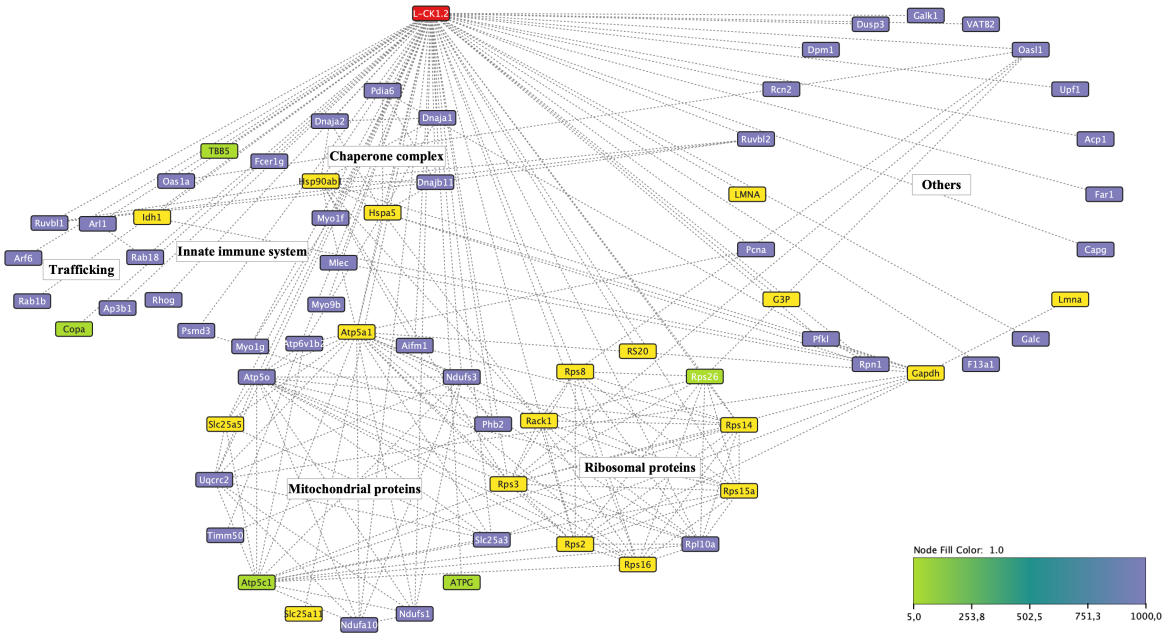
L-CK1.2
Chaperone complex
Trafficking
Innate immune system
Mitochondrial proteins
Ribosomal proteins
Others
Node Fill Color: 1.0
5,0
253,8
502,5
751,3
1000,0

C

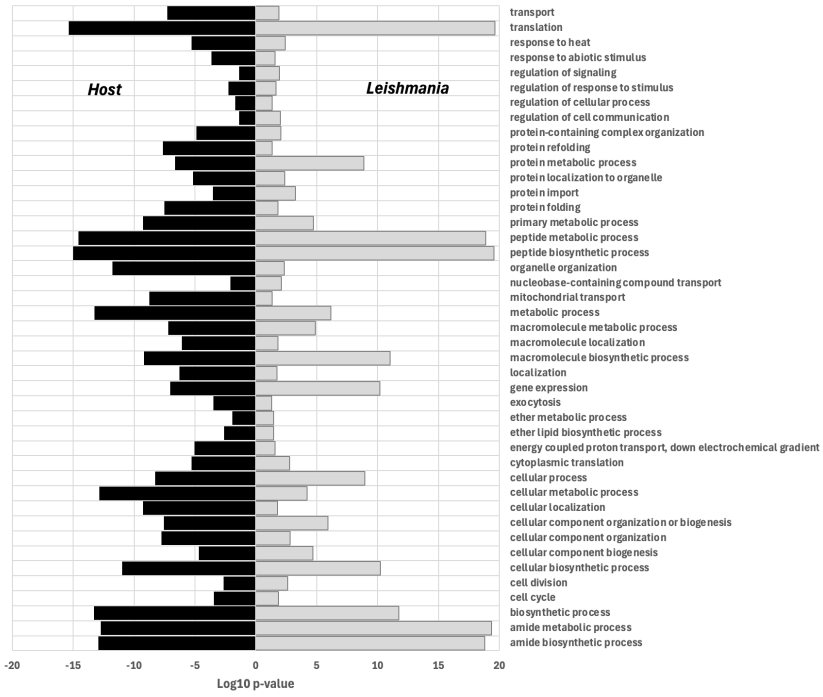
Host
Leishmania
transport
translation
response to heat
response to abiotic stimulus
regulation of signaling
regulation of response to stimulus
regulation of cellular process
regulation of cell communication
protein-containing complex organization
protein refolding
protein metabolic process
protein localization to organelle
protein import
protein folding
primary metabolic process
peptide metabolic process
peptide biosynthetic process
organelle organization
nucleobase-containing compound transport
mitochondrial transport
metabolic process
macromolecule metabolic process
macromolecule localization
macromolecule biosynthetic process
localization
gene expression
exocytosis
ether metabolic process
ether lipid biosynthetic process
energy coupled proton transport, down electrochemical gradient
cytoplasmic translation
cellular process
cellular metabolic process
cellular localization
cellular component organization or biogenesis
cellular component organization
cellular component biogenesis
cellular biosynthetic process
cell division
cell cycle
biosynthetic process
amide metabolic process
amide biosynthetic process
-20
-15
-10
-5
0
5
10
15
20
Log10 p-value

Figure 6

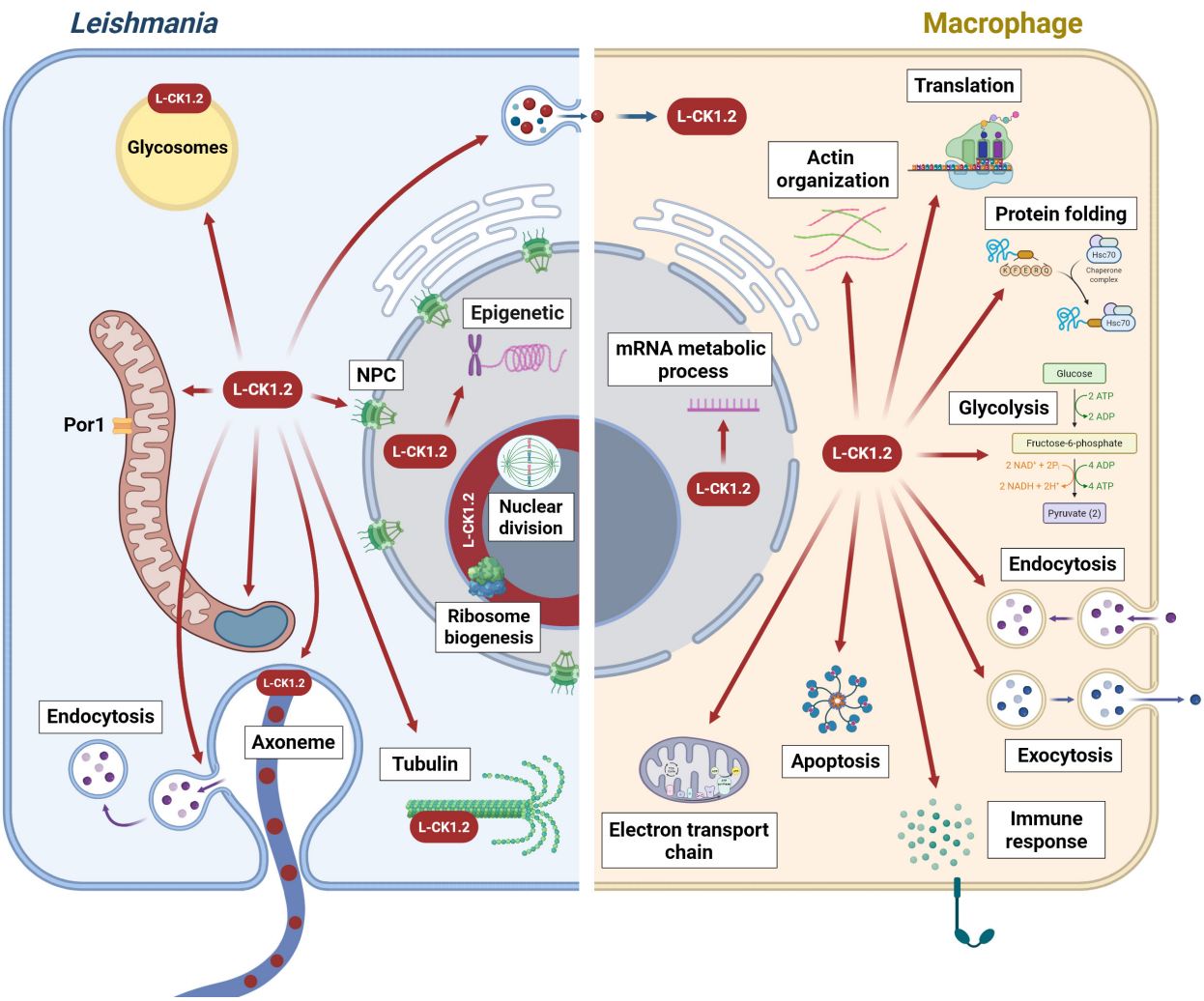
Leishmania
Macrophage
L-CK1.2
Glycosomes
Por1
NPC
Epigenetic
Nuclear division
Ribosome biogenesis
Endocytosis
Axoneme
Tubulin
Translation
Actin organization
Protein folding
Hsc70
Chaperone complex
mRNA metabolic process
Glycolysis
Glucose
2 ATP
2 ADP
Fructose-6-phosphate
4 ADP
4 ATP
Pyruvate (2)
Endocytosis
Exocytosis
Apoptosis
Electron transport chain
Immune response